Fourier-transform method for accurate analysis of Mössbauer spectra

J. G. Mullen and A. Djedid
Department of Physics, Purdue University, West Lafayette, Indiana 47907

G. Schupp, D. Cowan, Y. Cao, and M. L. Crow
Department of Physics, University of Missouri, Columbia, Missouri 65211

W. B. Yelon
Research Reactor, University of Missouri, Columbia, Missouri 65211
(Received 3 August 1987)

We report a simple analytic form for the convolution integral in transmission Mössbauer spectroscopy allowing accurate representation of the line shape even for very thick absorbers ($t=10$), and permitting easy fitting to the true line-shape function. This representation permits the accurate determination of all Mössbauer-effect (ME) parameters, including position, width, cross section, and interference. This analytic method can be applied to deconvolute accurately information contained in either source or absorber, and an explicit analytic form for the emission and absorption Fourier transforms is given. We show that from the asymptotics of the line shape, it is possible to determine all line-shape parameters, and that line-shape asymptotics can circumvent short-ranged hyperfine or instrumental broadening contributions to the observed spectrum. A formula for the correction to the line shape caused by source self-absorption is given, and it is shown that when there is significant source resonance self-absorption a "good" fit to data, judged by a chi-squared analysis, can yield completely wrong ME line-shape parameters. We find an equation for the dependence of the area under the absorption curve and the resonance peak height, and give its explicit dependence on the interference parameter and source broadening parameters. Although these effects have been neglected in earlier work, their contribution may be of order 10% in many cases of interest.

I. INTRODUCTION

From the earliest days of Mössbauer-effect (ME) spectroscopy it was recognized that the intrinsic shape of the emission line was a Breit-Wigner or Lorentzian function. When the emission spectrum is convoluted with the absorption spectrum in a transmission experiment, the observed ME pattern ideally is a shape, in the absence of hyperfine structure or interference effects, which is described by

$$A(x)=A(\infty)+C(x^2+1)^{-1}\ , \tag{1}$$

where x is a dimensionless gauge of the relative energy (Doppler velocity) shift, and is given by

$$x=(E-E_r)\tau/\hbar=(v-v_0)E_0\tau/\hbar c\ . \tag{2}$$

E_0 is the energy of the ME transition and is very large in magnitude compared to any of the other energy terms, E_r is the relative chemical and thermal shift of the absorber compared with the source, and E is the Doppler shift in energy resulting from the source motion relative to the absorber. The Doppler velocity representing the shift from the resonance peak is $v-v_0$, and is proportional to the energy shift in accordance with Eq. (2). v_0 is the Doppler velocity corresponding to the difference in transition energy of absorber compared to source, taken as positive when the absorber moves toward the source. C and $A(\infty)=A_0$ are constants gauging the size of the ME spectrum and the off-resonance (photoelectric absorption) count rate registered through the resonance absorber, respectively. $\hbar$ is Planck's constant divided by 2π, and c is the velocity of light. We summarize the definitions and often repeated relations in Appendix A of this paper for easy reference.

We shall make our analysis based on the use of a monochromating crystal filter, such as shown in Fig. 1, and we assume that the geometry of collimation and the Debye-Waller factor for the crystal used is such that the number of recoilless photons incident on the scattering crystal is the same as that leaving this crystal. Thus the only nonresonant gamma rays received by the crystal are those associated with the ME transition. The zero-phonon transitions are called recoilless and the one-or-more phonon processes are classified collectively as the nonresonant radiation. In general one will have other nonresonance radiation associated with other higher energy transitions in the source. For simplicity of exposition we take a geometry where these have been filtered out, although there is no difficulty in including them in the analysis.

In Fig. 2 we display the notation associated with the various count rates that register at the detector in an experiment using the transmission geometry shown in Fig. 1.

It was soon noted[1] after the discovery of the ME that for finite thickness absorbers Eq. (1) was not a good representation of real ME lines, and several researchers[2–10]

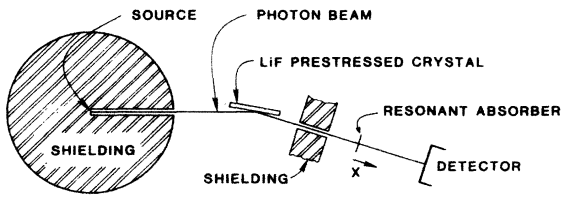

FIG. 1. Schematic drawing of a ME transmission experiment using a LiF crystal as a monochromating crystal to select the ME transition. With good shielding such a filter will suppress almost all radiation from the gamma detector except for the ME transition which will have two components: the zero-phonon part and the one- and multiphonon part.

have contributed to the analysis of line-shape modifications that result from saturation effects that are always inherent in real ME experiments, where the absorber thickness number is typically far from the thin limit, and in many cases the source resonance self-absorption (SRSA) significantly modifies the ME line shape.

Even in the ideal thin limit where there are no sources of broadening, the line shape is generally altered because of dispersive effects, resulting from interference between Rayleigh and nuclear resonance scattering and between photoelectrons and conversion electrons. These dispersive effects modify Eq. (1), giving it the form

$$A(x)=A_0+C(1-2\beta x)L(x)\ , \tag{3}$$

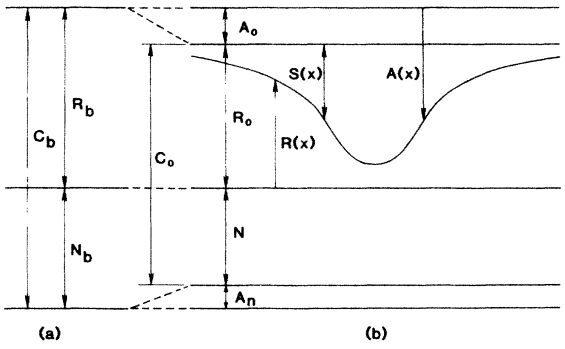

FIG. 2. Schematic representation of the resonant, $R(x)$, and nonresonant, N, gamma radiation received at the detector: (a) when there is no resonance absorber in the beam, and (b) when there is a resonance absorber moving at reduced velocity x with respect to the source. $S(x)$ is the observed signal which is measured against the off-resonance background C_0. C_b is the count rate when the absorber foil is absent and C_0 is the off-resonance count rate when the absorber is present. $A(x)$ represents the absorption of resonance radiation and A_n the absorption of nonresonance radiation. The off-resonance count rate of the resonance radiation is $R_0=R(\infty)$. This recoilless component of the count rate will be reduced as self-absorption becomes significant ($t_{rs}\gtrsim 0.05$) and R_0 will be reduced by a factor ρ defined in Eq. (31) of text.

where $L(x)$ is the Lorentzian function

$$L(x)=(x^2+1)^{-1}\ . \tag{4}$$

For notational brevity we shall define the product in Eq. (3) as

$$\mathcal{L}(x)=(1-2\beta x)L(x)\ . \tag{5}$$

The magnitude of the dispersive term β, called the interference parameter has been calculated by Goldwire and Hannon[11] and by Davis, Koonin, and Vogel[12] for many ME transitions. The importance of this term in ME time-reversal experiments has been discussed by Hannon and Trammell.[13]

In this paper we present an analysis of saturation effects in transmission experiments that includes source self-absorption and interference contributions to the line shape. In addition to giving a simple analytic expression for the transmission line shape we give formulas for the Fourier transforms of source and absorption terms arising in the convolution integral. The latter have use in the problem of deconvolution of ME spectra. Numerical approaches to Fourier deconvolution have been discussed by several authors,[14–16] and an analytic expression for both the source and absorber line-shape Fourier transforms greatly augments these techniques for deconvolution, making the extraction of the physics from ME measurements more precise and free of anomalies associated with the necessary divisions by source or absorber Fourier transforms in the deconvolution procedure.

II. THE TRANSMISSION CONVOLUTION INTEGRAL

When a transmission experiment is carried out in the geometry of Fig. 1, the photons transmitted to the detector are attenuated by the absorbing foil as a function of its reduced velocity x. Denoting $w_s(x)$ as the spectral distribution of recoilless photons emitted by the source and reflected by the LiF filter, the absorption from the beam is described by

$$A(x)=C_b\int_{-\infty}^{\infty} w_s(x-x')g_1(x')dx'\ , \tag{6}$$

where we take C_b as the count rate at the detector before the absorber is placed in the beam, and is equal to the recoilless plus nonrecoilless count rates, i.e., R_b+N_b as shown in Fig. 2(a). T_{ea} is the number of characteristic absorption lengths for electronic absorption (primarily photoelectric), and $g_1(x')$ is an absorption function, which convolutes with the source spectral distribution to give the observed ME line, which is described by

$$g_1(x')=1-\exp\{-[t\mathcal{L}(2x')+T_{ea}]\}\ , \tag{7}$$

where t is the number of characteristic absorption lengths in the absorber for the resonance radiation at the resonance maximum ($x=0$).

In addition to the absorption of recoilless (zero phonon) radiation [Eq. (6)] there will be an absorption of nonrecoilless radiation, A_n, which is independent of the reduced velocity x and is given by

$$A_n=[1-\exp(-T_{ea})]N_b$$
$$=(1-f_s)[1-\exp(-T_{ea})]C_b=(1-f_s)(C_b-C_0)\ , \tag{8}$$

where C_0 is the off-resonance count rate ($x \gg 1$) after the absorber is in place.

From the identity

$$g_1(x')=1-\exp(-T_{ea})+\exp(-T_{ea})$$
$$-[\exp(-T_{ea})]\{\exp[-t\mathcal{L}(2x')]\}\ , \tag{9}$$

we may remove the electronic absorption from the problem, i.e.,

$$A(x)=f_sC_b[1-\exp(-T_{ea})]$$
$$+[\exp(-T_{ea})]C_b\int_{-\infty}^{\infty}w_s(X)g(x')dx' \tag{10}$$
$$=A_0+C_0\int_{-\infty}^{\infty}w_s(X)g(x')dx'\ , \tag{11}$$

where A_0 is the off resonance absorption. We have adopted the notation that the Doppler shifted relative velocity of the source spectral maximum with respect to the absorber maximum is

$$X=x-x'\ , \tag{12}$$

with the absorption term given by

$$g(x')=1-\exp[-t\mathcal{L}(2x')]\ , \tag{13}$$

and we take the emission probability sum to normalize to the recoilless fraction emitted in the beam direction, f_s, i.e.,

$$\int_{-\infty}^{\infty}w_s(x)dx=f_s\ . \tag{14}$$

Notice that at the resonance peak for large t, the resonance absorption term $g(x')\rightarrow 1$, so that the second term in Eq. (11) is $f_sC_0=R_0$ as expected, i.e., the absorption rate at the resonance center is R_0, as all of the resonance photons transmitted at $x=\infty$ are absorbed at $x=0$ in this high-absorption limit. When there is insignificant resonance self-absorption in the source, the normalization factor on the right side of Eq. (14) will be set equal to f_{s0}, where f_{s0} is the recoilless fraction of radiation leaving the source in the beam direction, which is the usual meaning of recoilless fraction, and f_s is the recoilless fraction leaving the source with resonance self-absorption by the source, which is always less than f_{s0}. For the cases we will consider the resonance self-absorption reduction factor $\rho=f_s/f_{s0}$ is typically between 0.9 and 1.0. As we explain in Sec. VII, good line-shape experiments should avoid sources where this ratio is less than 0.9, even though such cases could be dealt with by the methods given in this paper.

The first term in Eq. (11) is a constant A_0 representing the off-resonance absorption (principally photoelectric) and the second term is the measured resonance signal. This signal in transmission experiments is given by the convolution of source and absorption spectral distributions. Having factored out the dependence on T_{ea}, we write

$$S(x)=C_0\int_{-\infty}^{\infty}w_s(X)\{1-\exp[-t\mathcal{L}(2x')]\}dx'\ . \tag{15}$$

In this paper we shall calculate $w_s(x)$ including source resonance self-absorption (SRSA) for uniform sources, give analytic expressions for $S(x)$ to order β^2, and give analytic expressions for the Fourier transforms of the source and absorption terms, which can be used in the deconvolution of source from absorber spectral distributions.

III. SPECTRAL DISTRIBUTION OF A SOURCE WITH SELF-ABSORPTION

The time Fourier transform of the exponential decay law for a nuclear level leads to a Lorentzian line shape having a width $\hbar/\tau$, where τ is the mean life of the ME nuclear level. Using the same notation as given in Eq. (2) to describe the absorption line, the emission spectral distribution in the absence of resonance self-absorption is

$$w_s(x)=C_s[1+(2x)^2]^{-1}=C_sL(2x)\ , \tag{16}$$

where the factor $2x$ in the Lorentzian function arises from the fact that the level width is only half of the ideal convoluted width observed in an ME experiment. Some authors use the half-level width to set the gauge of the dimensionless reduced velocity (see Ref. 5 as an example). We prefer the above form as it leads to simpler expressions in the final results and because experimentalists usually use the full-level width, or half the ideal ME width, in the discussion of data.

It is general practice to use a Lorentzian for the source distribution, as given in Eq. (16), although it is in many cases grossly in error as we shall show. As a source decays there is an inevitable production of its daughter nuclei. As the decay continues there is a progressive build-up of resonance self-absorption, resulting in an ever increasing broadening in the emission spectral distribution and distortion in the line shape.

The effect of source resonance self-absorption (SRSA) is easily calculated. Consider the uniform source illustrated in Fig. 3. If we sum the contributions to absorption for each small element of thickness dn, we find for a uniform source that the resulting spectral distribution is given by

$$w_s(x)=\frac{C_s}{n_s}\int_0^{n_s}L(2x)\exp\{-[\sigma_{rs}(x)+\sigma_{es}]n\}dn\ , \tag{17}$$

or after integration

$$w_s(x)=C_sL(2x)[1-\exp(-t_s)]/t_s\ , \tag{18}$$

where

$$t_s=t_{rs}\mathcal{L}(2x)+T_{es}\ . \tag{19}$$

The quantities used in Eqs. (17) through (19) not previously defined are as follows:

$$\sigma_{rs}(x)=f_s\sigma_0a_{s1}\mathcal{L}(2x)\ , \tag{20}$$

$$\sigma_{es}=\sum_{i=1}^{N_s}\sigma_{ei}a_{si}\ , \tag{21}$$

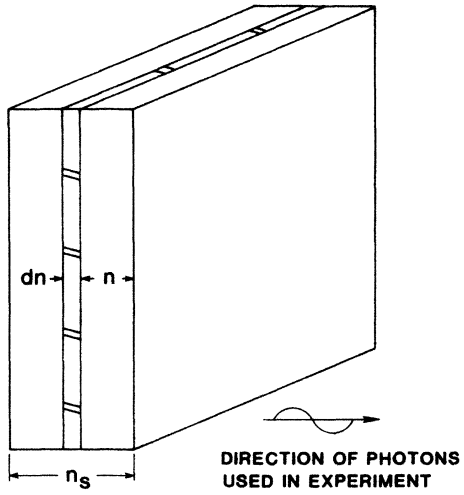

FIG. 3. Sketch of a uniform source with an imaginary section parallel to the face. ME photons in the beam direction are absorbed by n atoms/cm^2 of which $a_{s1}n_s$ resonantly absorb the emission line, both broadening and modifying the shape of the line.

σ_{ei} is the electronic cross section associated with the ith type atom, a_{s1} is the fraction of source atoms of the ME type, and a_{si} is the fraction of source atoms of species i. n_s is the total number of atoms per unit area of all types of atoms in the source,

$$t_s=[\sigma_{rs}(x)+\sigma_{es}]n_s \ ,$$

t_{rs} is the number of characteristic thicknesses in the source for resonance absorption, $f_{s0}\sigma_0 a_{s1}n_s$, and T_{es} is the number of characteristic thicknesses in the source for nonresonance electronic absorption, $\sigma_{es}n_s$.

In order to calculate the Fourier transform of the source distribution function, it is necessary to expand Eq. (18) in a power series. Thus,

$$w_s(x)=C_s L(2x)\sum_{m=1}^{\infty}(-1)^{m+1}(m!)^{-1}t_s^{m-1} \ . \tag{22}$$

If we also expand t_s using binomial coefficients, we have

$$w_s(x)=C_s\sum_{m=1}^{\infty}\sum_{k=0}^{m-1}(-1)^{m+1}(m!)^{-1}\binom{m-1}{k}T_{es}^{m-1-k} \times t_{rs}^k L(2x)\mathcal{L}^k(2x) \ . \tag{23}$$

If we define

$$E_k(T_{es})=\sum_{m=k+1}^{\infty}(-1)^{m+1}(m!)^{-1}\binom{m-1}{k}T_{es}^{m-1-k} \ , \tag{24}$$

and make the replacement

$$\sum_{m=1}^{\infty}\sum_{k=0}^{m-1}\rightarrow\sum_{k=0}^{\infty}\sum_{m=k+1}^{\infty} \ , \tag{25}$$

Eq. (23) can be written in the form

$$w_s(x)=C_s\sum_{k=0}^{\infty}E_k(T_{es})t_{rs}^k L(2x)\mathcal{L}^k(2x) \ . \tag{26}$$

Good line-shape measurements are much simpler with thin sources, although it is often impractical to use sources that have negligible self-absorption, and which are well represented by only the leading term ($k=0$) of Eq. (23). For high intensity sources like ^{183}Ta, which we have fabricated by neutron irradiation at the University of Missouri Research Reactor, we choose the thickness of our ^{181}Ta foil such that $T_{es}\cong 1$. After a 1-week irradiation t_{rs} is of order 0.03 and after a 2-week irradiation and subsequent decay, t_{rs} may approach 0.3, depending on location in the flux trap and local flux magnitude. For sources where $t_{rs}=0.5$, it is desirable to take at least one and preferably two or even three terms in Eq. (26) beyond $k=0$, which is the simple Lorentzian form occurring when SRSA is negligible.

Defining

$$\tau_k(T_{es})=E_k(T_{es})/E_0(T_{es}) \ , \tag{27}$$

the source distribution is given to third order by

$$w_s(x)=C_s E_0 L(2x)[1+\tau_1 t_{rs}\mathcal{L}(2x)+\tau_2 t_{rs}^2\mathcal{L}^2(2x)+\tau_3 t_{rs}^3\mathcal{L}^3(2x)] \ . \tag{28}$$

To show how sensitive the spectral distribution is to the number of resonance thicknesses of the source, we show in Fig. 4 the source distribution function given by Eq. (18) for $T_{es}=1$, $t_{rs}=0$ and 0.5, and compare the latter case with the linear approximations given by the first two terms of Eq. (28). Note how the peak of the distribution is very flattened, while the wings are relatively unaffected by SRSA. This is the result of the condition that the source absorbing nuclei are stationary with respect to the source emitting nuclei and cause maximum resonance absorption at the peak. Figure 4(c) shows the linear ap-

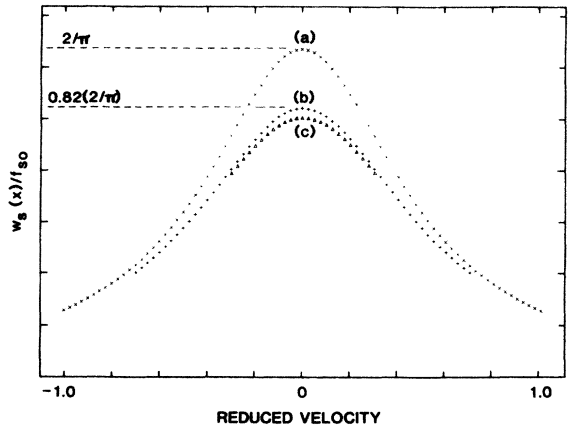

FIG. 4. Plots of the source distribution function $w_s(x)/f_{s0}$ for (a) $T_{es}=1$, $t_{rs}=0$ by direct numerical evaluation of Eq. (18); (b) $T_{es}=1$, $t_{rs}=0.5$ by direct numerical evaluation of Eq. (18); and (c) $T_{es}=1$, $t_{rs}=0.5$ by direct numerical evaluation of Eq. (28), using only the linear t_{rs} correction for source broadening. The second-order correction is almost indistinguishable from curve (b) on the scale shown.

proximation in t_{rs} to the source distribution. The quadratic approximation cannot be distinguished from the exact distribution within the accuracy of the plot.

The normalization constant in Eq. (26) is given by the normalization condition [Eq. (14)], i.e.,

$$\int_{-\infty}^{\infty} w_s(x)dx = (\pi/2)C_s E_0 \rho = f_{s0}\rho = f_s \ , \tag{29}$$

or

$$C_s E_0 = (2/\pi) f_{s0} \ , \tag{30}$$

where the reduction factor ρ is obtained by the integration of Eq. (26) term by term, using the method of residues, and neglecting terms of order $\tau_2 t_{rs}^2 \beta^2$, i.e.,

$$\rho = \sum_{k=0}^{\infty} 4^{-k}[(2k!)/(k!)^2]\tau_k t_{rs}^k \ . \tag{31}$$

To third order in source resonance thickness number, t_{rs}, we have

$$\rho = 1 + \tfrac{1}{2}\tau_1 t_{rs} + \tfrac{3}{8}\tau_2 t_{rs}^2 + \tfrac{5}{16}\tau_3 t_{rs}^3 \ . \tag{32}$$

For $T_{es}=1$, $t_{rs}=0.5$, $\rho=0.91$. Of course, in the absence of SRSA $t_{rs}=0$, whence $\rho=1$.

IV. FOURIER TRANSFORMS OF THE SOURCE AND ABSORBER FUNCTIONS

Using the emission distribution described by Eq. (28) the basic transmission integral [Eq. (15)] can be written in the form

$$S(x) = \frac{2}{\pi} f_{s0} C_0 \left[\int_{-\infty}^{\infty} L(2X) g(x')dx' + \tau_1 t_{rs} \int_{-\infty}^{\infty} L(2X)\mathcal{L}(2X) g(x')dx' \right.$$
$$\left. + \tau_2 t_{rs}^2 \int_{-\infty}^{\infty} L(2X)\mathcal{L}^2(2X) g(x')dx' + \tau_3 t_{rs}^3 \int_{-\infty}^{\infty} L(2X)\mathcal{L}^3(2X) g(x')dx' + \cdots \right] , \tag{33}$$

where we note that in the limit of large resonance self-absorption, where $t \to \infty$, $g \to 1$ and $S(0) = f_{s0} C_0 \rho = f_s C_0 = R_0$, that is, the resonance signal in this limit is R_0 and all of the resonance photons are absorbed.

We shall focus on the four leading integrals, which are explicitly displayed in Eq. (33). If the source thickness number is not greater than about 0.5, the signal $S(x)$ is well described by the terms given in Eq. (33). Good lineshape experiments require good count statistics and make high-intensity sources very desirable. For sources produced by neutron irradiation this means that we want the thickness of the source to be as great as possible, consistent with permissible electronic (primarily photoelectric) absorption. Thus $T_{es}=1$ is the norm for such sources. τ_k is a very slowly varying, nearly linear function as can be seen by the direct evaluation of Eq. (27) using Eq. (24). If we use a linear approximation and require the values of τ_k at $T_{es}=0$ and $T_{es}=1$ be exact, then τ_k's dependence on T_{es} can be approximately represented by

$$\tau_1(T_{es}) = -0.5 + 0.082 T_{es} \ ,$$
$$\tau_2(T_{es}) = 0.167 - 0.040 T_{es} \ , \tag{34}$$

and

$$\tau_3(T_{es}) = -0.0417 + 0.0117 T_{es} \ .$$

In most experiments the source thickness is constant and exact evaluation of $\tau_k(T_{es})$ for these cases is without difficulty. Equation (34) above is used here only for stressing the magnitude of these terms and their relative insensitivity to the precise electronic absorption thickness number T_{es}.

The convolution integrals of Eq. (33), are expressible in terms of Fourier transforms, which lead to a rapidly convergent truncation procedure. To calculate these transforms requires an expansion of the absorption function $g(x')$ in a power series, i.e.,

$$g(x') = \sum_{m=1}^{\infty} (-1)^{m+1}(m!)^{-1} t^m \mathcal{L}^m(2x') \ . \tag{35}$$

Continuing Eqs. (35) and (33) we can write the general resonance transmission signal as

$$S(x) = \frac{2}{\pi} f_{s0} C_0 \sum_{m=1}^{\infty} \sum_{k=0}^{\infty} (-1)^{m+1}(m!)^{-1} t^m \tau_k(t_{rs}^k) I_{km} \ , \tag{36}$$

where

$$I_{km} = \int_{-\infty}^{\infty} L(2X)\mathcal{L}^k(2x)\mathcal{L}^m(2x')dx' \ . \tag{37}$$

While this integral and the corresponding sum in Eq. (36) converges rapidly in k for moderate source self-absorption, the convergence in m is poor for typical ME absorption thickness number of 4. Application of the convolution theorem organizes terms that contribute to the integral in such a way that the sums on m are easily performed. Rewriting Eq. (37), we have

$$I_{km} = \frac{1}{4^{m+k+1}} \int_{-\infty}^{\infty} \frac{(1-4\beta X)^k (1-4\beta x')^m dx'}{(X^2+1/4)^{k+1}(x'^2+1/4)^m} \ . \tag{38}$$

If we expand the numerator of the source term to the linear term in β, the error will be only of order $\tau_2 t_{rs}^2 \beta^2$, or of order 10^{-3} even for the most unfavorable case. Expanding the absorption term to order β^2 again limits the errors to about 10^{-3}. The source and absorption Fourier transforms are then

$$F_k^{(0)}(\alpha) = \frac{1}{4^{k+1}} \int_{-\infty}^{\infty} \frac{e^{-i\alpha x} dx}{(x^2+1/4)^{k+1}} \ , \tag{39}$$

and

$$F_k^{(1)}(\alpha)=\frac{-4\beta k}{4^{k+1}}\int_{-\infty}^{\infty}\frac{xe^{-i\alpha x}dx}{(x^2+1/4)^{k+1}}$$
$$=-4\beta k\left[i\frac{d}{d\alpha}F_k^{(0)}(\alpha)\right], \tag{40}$$

where the first-order transform which is linear in β is easily solved by differentiation with respect to α of the solution to Eq. (39). The superscript (0), (1), and (2) mean zeroth-, first-, and second-order terms with respect to interference parameter β throughout this paper.

The Fourier transforms of the absorption term in Eq. (38) for the zeroth, first, and quadratic β terms in Eq. (40) are

$$G_m^{(0)}(\alpha)=\frac{1}{4^m}\int_{-\infty}^{\infty}\frac{e^{-i\alpha x}dx}{(x^2+1/4)^m}, \tag{41}$$

$$G_m^{(1)}(\alpha)=-4\beta m\left[i\frac{d}{d\alpha}G_m^{(0)}(\alpha)\right], \tag{42}$$

and

$$G_m^{(2)}(\alpha)=8\beta^2 m(m-1)\left[i\frac{d}{d\alpha}G_m^{(1)}(\alpha)\right]. \tag{43}$$

Again the higher-order terms follow directly from the zeroth order, represented by the solution to Eq. (41). The formal similarity between Eqs. (41) and (39) means that the solution to Eq. (39) will immediately give the solution to Eq. (41). Thus all of the relevant Fourier transforms will immediately follow when Eq. (39) is solved.

The Fourier transform in Eq. (39) can be evaluated by the method of residues. For positive α, $F_+^{(0)}(\alpha)$ can be found by closing the contour of integration on the lower half plane, and $F_-^{(0)}(\alpha)$ by closing on the upper half plane. Writing the integral in Eq. (39) in terms of the complex variable we enclose poles of order k at $-i/2$ in the lower half plane. Thus we have

$$F_{k+}^{(0)}(\alpha)=-\frac{1}{4^{k+1}}\oint\frac{e^{-i\alpha z}}{(z+i/2)^{k+1}(z-i/2)^{k+1}}$$
$$=-\frac{2\pi i}{k!}(uv)^{(k)}\Big|_{z=-i/2}$$
$$=-\frac{2\pi i}{k!}\sum_{p=0}^{k}\binom{k}{p}u^{(p)}v^{(k-p)}\Big|_{z=-i/2} \tag{44}$$

where the superscripts on u and v refer to the order of derivative with respect to z and where the functions are evaluated at the pole with u and v defined by

$$u(z)=(z-i/2)^{-(k+1)}$$
and
$$v(z)=e^{-i\alpha z}. \tag{45}$$

Carrying out the indicated differentiations and evaluating at the poles yields the required transform, i.e.,

$$F_{k\pm}^{(0)}(\alpha)=\frac{1}{4^{k+1}}\frac{2\pi}{k!}\sum_{p=0}^{k}\frac{(-2)^{k-p}(k+p)!}{p!(k-p)!}\times(\mp\alpha/2)^{k-p}\exp(\mp\alpha/2), \tag{46}$$

where the result for $F_{k-}^{(0)}$ has been included and follows by the same analysis, but with the pole at $+i/2$ used to evaluate the residue when closure is carried out in the upper half plane.

When there is no SRSA the only F term required is for $k=0$. Most of the physics is contained in this term. We give $F_{k\pm}^{(0)}$ for $k=0$, 1, 2, and 3, in Table I, which are all even parity functions, and the odd parity derivative $F_{k\pm}^{(1)}(\alpha)$ for $k=1$, 2, and 3. These are sufficient terms to yield an excellent representation of the signal $S(x)$, for sources having a resonance thickness number $t_{rs}\leq 0.5$.

Applying the same procedure to calculate $G_{m\pm}^{(0)}(\alpha)$, i.e., substituting $m-1$ for k we find after replacing the index p by $m-j$

$$G_{m\pm}^{(0)}(\alpha)=4^{-m}\sum_{j=1}^{m}C_{jm}(\mp\alpha/2)^{j-1}\exp(\mp\alpha/2), \tag{47}$$

$$C_{jm}=\frac{(2\pi)(-2)^{j-1}(2m-j-1)!}{(m-1)!(m-j)!(j-1)!}. \tag{48}$$

The linear and quadratic terms in the absorption transforms follow from Eq. (47) by direct differentiation using Eqs. (42) and (43), and they are summarized in Table I. Notice that the transforms are written in a particular form, which allows the signal $S(x)$ to be read off immediately by the power of $(\mp\alpha/2)$ associated with the various transform products required for each contribution to $S(x)$.

V. RESONANCE SIGNAL IN THE ABSENCE OF SOURCE BROADENING AND INTERFERENCE

By taking the inverse transform of $F_{k\pm}^{(0)}G_{m\pm}^{(0)}$ we obtain the term I_{0m} in Eq. (38) and an expression for the resonance signal as prescribed by Eq. (36). We have

$$I_{0m}^{(0)}(x)=4^{-m-1}\sum_{j=1}^{m}C_{jm}\mathcal{J}_j(x), \tag{49}$$

where the superscript on I gives the order in β that the integral represents, where $\mathcal{J}_j(x)$ is the integral

$$\mathcal{J}_j(x)=\int_{-\infty}^{0}(\alpha/2)^{j-1}\exp[i\alpha x+\alpha(w+1)/2]d\alpha$$
$$+\int_{0}^{\infty}(-\alpha/2)^{j-1}\exp[i\alpha x-\alpha(w+1)/2]d\alpha. \tag{50}$$

Note that the exponential has been modified by replacing α in the second term of the argument of the exponential with $\alpha(w+1)/2$. The reason for introducing this factor is primarily to permit the use of a recursion relation that is a helpful tool in evaluating the integral for successive j values and to permit the result to be expressed in a natural way as a simple polynomial in powers of $L(x)$, which is easily programmed onto a computer. Also, it should be noted that this width parameter, w, arises natu-

TABLE I. Fourier transforms used to describe ME line-shape to second order in β and third order in t_{rs}. C_{jm} is given in Eq. (48) of text.

$$F^{(0)}_{0\pm}(\alpha)=2\pi(\tfrac{1}{4})\exp(\mp\alpha/2)$$
$$F^{(0)}_{1\pm}(\alpha)=2\pi(\tfrac{1}{8})[1-(\mp\alpha/2)]\exp(\mp\alpha/2)$$
$$F^{(1)}_{1\pm}(\alpha)=2\pi(\beta/2)[(\mp i/2)(\mp\alpha/2)]\exp(\mp\alpha/2)$$
$$F^{(0)}_{2\pm}(\alpha)=2\pi(\tfrac{1}{32})[3-3(\mp\alpha/2)+(\mp\alpha/2)^2]\exp(\mp\alpha/2)$$
$$F^{(1)}_{2\pm}(\alpha)=2\pi(-\beta/4)[-(\mp i/2)(\mp\alpha/2)+(\mp i/2)(\mp\alpha/2)^2]\exp(\mp\alpha/2)$$
$$F^{(0)}_{3\pm}(\alpha)=2\pi(\tfrac{1}{192})[15-15(\mp\alpha/2)+6(\mp\alpha/2)^2-(\mp\alpha/2)^3]\exp(\mp\alpha/2)$$
$$F^{(1)}_{3\pm}=2\pi(-\beta/16)[-3(\mp i/2)(\mp\alpha/2)+3(\mp i/2)(\mp\alpha/2)^2-(\mp i/2)(\mp\alpha/2)^3]\exp(\mp\alpha/2)$$
$$G^{(0)}_{m\pm}(\alpha)=4^{-m}\sum_{j=1}^{m}C_{jm}(\mp\alpha/2)^{j-1}\exp(\mp\alpha/2)$$
$$G^{(1)}_{m\pm}(\alpha)=(-4m)4^{-m}\sum_{j=1}^{m}C_{jm}[(\mp i/2)(\mp\alpha/2)^{j-1}+(j-1)(\mp i/2)(\mp\alpha/2)^{j-2}]\exp(\mp\alpha/2)$$
$$G^{(2)}_{m\pm}(\alpha)=-[2m(m-1)\beta^2]4^{-m}\sum_{j=1}^{m}C_{jm}[(\mp\alpha/2)^{j-1}+2(j-1)(\mp\alpha/2)^{j-2}+(j-1)(j-2)(\mp\alpha/2)^{j-3}]\exp(\mp\alpha/2)$$

rally if we replace the factors $(\frac{1}{2})^2$ in the denominators of integrals of Eq. (38) by $(w/2)^2$. Thus, this parameter can serve as a natural way for generalizing to the case of intrinsically broadened Lorentzians such as have been proposed when ME lines are diffusion broadened. We will not consider this latter case in this paper and will always taken $w=1$ in all final results. For the purpose of this paper w is merely a parameter which facilitates the evaluation of the higher order items in Eq. (50) and, subsequently, Eq. (71) as a polynomial in powers of Lorentzians.

There are two alternative ways of evaluating the integrals in Eq. (50), and we shall examine both of these approaches. The first of these involves formulating a recursion relation for successively higher terms in j, which can be generated by taking derivatives with respect to x of lower $\mathcal{J}_j$ terms, and the second involves developing a recursion in terms of derivatives with respect to w. When the first approach is used the width factor w introduced in Eq. (49) is superfluous and need not be introduced. There are some important aspects to be considered in both approaches and we will briefly discuss each method.

For $j=1$ Eq. (50) is an elementary integral and immediately evaluated, i.e.,

$$\mathcal{J}^{(0)}_1(x)=2L(x)\ . \tag{51}$$

Calling the first integral in Eq. (50) $\mathcal{J}_{j-}$ and the second one $\mathcal{J}_{j+}$, we see that

$$\mathcal{J}^{(0)}_{j+1}(x)=-\frac{i}{2}\frac{d}{dx}\mathcal{J}^{(0)}_{j-}(x)+\frac{i}{2}\frac{d}{dx}\mathcal{J}^{(0)}_{j+}(x)\ . \tag{52}$$

The lowest order even j term is then given by

$$\mathcal{J}^{(0)}_2(x)=-\frac{i}{2}\frac{d}{dx}\int_{-\infty}^{0}\exp(i\alpha x-\alpha)d\alpha + \frac{i}{2}\frac{d}{dx}\int_{0}^{\infty}\exp(i\alpha x+\alpha)d\alpha\ , \tag{53}$$

or, if we explicitly evaluate the integrals in Eq. (53), we find

$$\mathcal{J}^{(0)}_2(x)=-\frac{d}{dx}[xL(x)]\ , \tag{54}$$

which like $\mathcal{J}_1(x)$ is again an even function of x.

All j odd and even terms are simply related to $\mathcal{J}^{(0)}_1(x)$ and $\mathcal{J}^{(0)}_2(x)$, respectively. Thus, from Eq. (51) it follows immediately that

$$\mathcal{J}_{j+2}=-\tfrac{1}{4}\mathcal{J}''_j(x)\ , \tag{55}$$

where the double prime means the second derivative with respect to x. Expressing $\mathcal{J}_j$ in terms of the lowest odd and even terms given by Eqs. (51) and (53), respectively, yields

$$\mathcal{J}^{(0)}_j(x)=(-1)^{(j-1)/2}2^{2-j}\frac{d^j}{dx^j}L(x),\quad j=1,3,5\ldots\ , \tag{56}$$

$$\mathcal{J}^{(0)}_j(x)=(-1)^{j/2}2^{2-j}\frac{d^j}{dx^j}[xL(x)],\quad j=2,4,6\ldots\ . \tag{57}$$

Substituting Eqs. (56) and (57) for the integral, Eq. (50), we obtain an explicit functional dependence for $\mathcal{J}_j(x)$ in Eq. (49), which yields, when substituted into Eq. (33), the resonance signal in the absence of source broadening and interference, i.e.,

$$S^{(0)}(x)=f_{s0}C_0\sum_{j=1}^{\infty}D^{(0)}_j(t)d^{(0)}_j(x)\ , \tag{58}$$

where the capital D's are pure functions of the absorber thickness number t and the small d's are pure functions of the reduced velocity x, and in this case are equal to $\mathcal{J}_j(x)$. The explicit form of D_j for this case is

$$D^{(0)}_j(t)=\sum_{m=j}^{\infty}A_{jm}t^m\ , \tag{59}$$

with

$$A_{jm}=\frac{(-1)^{m+j}2^{j-1}(2m-j-1)!}{4^m m!(m-1)!(m-j)!(j-1)!}\ . \tag{60}$$

It is instructive to explicitly write out some of the terms of Eq. (58) to show the convergence and character of this expansion. To order $j=4$ we have

$$S^0(x)=f_{s0}C_0\sum_{m=1}^{\infty}\frac{(-1)^{m+1}(2m-2)!}{4^m m![(m-1)!]^2}t^m 2L(x)+\sum_{m=2}^{\infty}\frac{2(-1)^m(2m-3)!}{4^m m!(m-1)!(m-2)!}t^m\frac{d}{dx}[-xL(x)]$$
$$+\sum_{m=3}^{\infty}\frac{2^2(-1)^{m+1}(2m-4)!}{4^m m!(m-1)!(m-3)!2!}t^m\frac{d^2}{dx^2}[-\tfrac{1}{2}L(x)]+\sum_{m=4}^{\infty}\frac{2^3(-1)^m(2m-5)!}{4^m m!(m-1)!(m-4)!3!}t^m\frac{d^3}{dx^3}[\tfrac{1}{4}xL(x)]+\cdots . \tag{61}$$

Evaluation of the leading terms in each sum gives

$$S(x)=f_{s0}C_0\{(t/2-t^2/8+t^3/32-5t^4/768+\cdots)L(x)-(t^2/16-t^3/64+5t^4/1536-\cdots)[xL(x)]'$$
$$-(t^3/384-t^4/1536+\cdots)[L(x)]''+(t^4/18\,432-\cdots)[xL(x)]'''+\cdots\}, \tag{62}$$

where the primes on the square-bracketed quantities on the right refer to the number of derivatives with respect to x of the quantity inside the brackets.

At this point the value of the Fourier transform technique is clearly manifested. A brute force approach to the problem requires a prohibitive number of integrals to be of much interest. The Fourier transforms and their inverses give a way of partially evaluating the higher-order I_m's and organizing the terms in such a way as to yield a very rapidly converging series for the resonance signal $S^{(0)}(x)$. The slow convergence in m for large t is unimportant as this series is easily handled by even a modest computer. The rapid convergence in j is crucial and we shall be discussing this in greater detail later.

From Eqs. (58), (61), and (62) we can immediately draw several interesting conclusions. Since all of the terms have derivatives with respect to x times coefficients which are independent of x, except for the first, the first term alone will contribute to the total area, A_T, under the resonance curve. Thus, we immediately arrive at

$$A_T=f_{s0}C_0(2\pi)\sum_{m=1}^{\infty}A_{1m}t^m , \tag{63}$$

where A_{1m} is given by Eq. (60) with $j=1$.

This result can be shown by direct numerical calculation to agree with an earlier result derived by Bykov and Hien,[5] even though their result was expressed in terms of Bessel functions and arrived at by a completely different approach. It should be noted that the formula by Bykov and Hien gives results differing by a factor of 2 from ours due to a different choice of dimensionless units for the reduced velocity factor x. When care is taken to account for this difference in units, the results are identical. One advantage of the present analysis, as we shall show explicitly in Secs. VI and VII, is that we may easily include into the area calculation the effects of both source resonance self absorption and interference, as these are merely add-on terms to Eq. (63).

Each sum in Eqs. (61) and (62) represents successively higher j in Eq. (58), i.e., $j=1,2,3,\ldots$. Since successive terms of each of the power series sums in Eq. (58) can be expressed in terms of a simple recursion relation, i.e.,

$$A_{j,m+1}=-\frac{(2m+1-j)(2m-j)}{4m(m+1)(m+1-j)}A_{jm} . \tag{64}$$

A suitable cutoff on the ratio of $A_{jm}/A_{j,m+1}$ can be used to effect a sum to infinity while minimizing computational time.

We should mention here that the Fourier transform approach is what makes possible the rapid convergence of $S(x)$. The integrals arising in Eq. (33) can be directly evaluated by the method of residues without utilizing Fourier transforms. Unfortunately, the complete integrals do not lead to rapid convergence for large absorber thickness number, and they also do not yield a simple and general formula for the resonance signal. The Fourier transforms give a systematic way of truncating the higher order integrals so that the resulting series representing $S(x)$ is rapidly convergent, which allows this representation to be used for easy curve fitting to real transmission data. For example, taking an absorber thickness number of 8, twice that of a typical ME experiment, taking j up to 10 yields an error in $S(x)$ of only 20 ppm, well beyond even the most precise current experiments.

The derivatives of $L(x)$ and $xL(x)$ are well behaved, slowly varying functions and serve as a highly convergent basis set for describing saturation-broadened ME lines. The second function of the series $[xL(x)]'$, which is the leading function beyond the Lorentzian, is a W-shaped function shown in Fig. 5(c). It is interesting that authors[17] who have measured interference parameters, and who have dared to show their residual plot, do see a W signature, having essentially an identical pattern to the next term beyond the Lorentzian, which reveals the fundamental error of trying to fit data to Lorentzian functions when doing interference and precision line-shape determinations.

In the development given here, the recursion relations described by Eqs. (56) and (57) require partitioning into separate groups the j even and j odd terms. An alternative approach which leads to a single recursion relation is the usage of the width parameter w. This leads to a representation of the $d_j(x)$ in terms of powers of Lorentzians, and this form is very convenient for programming on the computer. From Eq. (50) it is immediately evident that an alternative recursion relation is

$$d_j^{(0)}(x)=\frac{\partial}{\partial w}d_{j-1}^{(0)}(x)\bigg|_{w=1}=\frac{\partial^{j-1}}{\partial w^{j-1}}d_{j-1}^{(0)}(x)\bigg|_{w=1} , \tag{65}$$

or

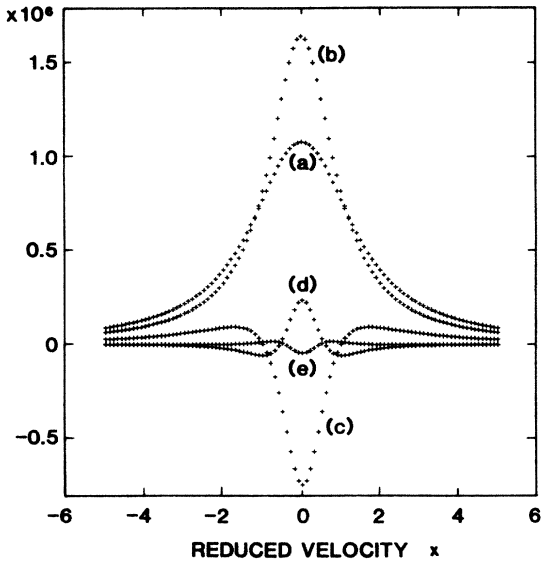

FIG. 5. (a) A plot of the numerically calculated $S^{(0)}_{\mathrm{CONV}}(x)$ for $t=4$, $R_0=(\pi/2)\times 10^6$, $t_{rs}=T_{es}=\beta=0$; (b), (c), and (d) are comparison plots of $S^{(0)}_j(x)$ for $j=1$, 2, and 3, respectively, showing the composite structure of the saturation broadened line. Plot of the difference in $S^{(0)}_{\mathrm{CONV}}(x)-S^{(0)}_{\mathrm{AN}}(x)$ when only the contributions from $j=1$, 2, and 3 are added, giving a maximum error signal at the origin of only 5%. S_{CONV} is a computer-generated data base using Eq. (15), with Eq. (18) for the source term and Eq. (13) for the absorption term.

$$d^{(0)}_j(x)=\frac{\partial^{j-1}}{\partial w^{j-1}}[(w+1)L_w]_0$$
$$=2L^{(j-1)}_{w0}+(j-1)L^{(j-2)}_{w0}\ , \tag{66}$$

where the superscript $j-1$ on the L terms means the $j-1$ partial derivative with respect to w and the 0 subscript means evaluated at $w=1$ after differentiation. Note that the second term in the last expression is not defined for $j=1$. L_w or $[x^2+(w+1)^2]^{-1}$ is simply the Lorentzian generalized to include the width parameter. When cases such as this occur the coefficient associated with that term is always zero, and in every instance where this occurs, that term should be taken as zero, since an examination of these cases show that the term in question does not in fact exist.

Evaluation of the first three of the functions expressed in Eq. (66) leads to

$$d^{(0)}_1(x)=2L(x)\ ,$$
$$d^{(0)}_2(x)=L(x)-2L^2(x)\ , \tag{67}$$

and

$$d^{(0)}_3(x)=-3L^2(x)+4L^3(x)\ ,$$

which, except for the first, appear quite different than the derivatives prescribed in Eqs. (56) and (57) and displayed in Eq. (61), although straightforward algebraic rearrangement confirms that they are equivalent. We shall use the second recursion approach [Eq. (65)] in subsequent development, because the even and odd terms do not have to be treated separately and because the $\mathcal{J}_j$ and $\mathcal{d}_j$ basis functions and the composite d functions calculated in this way are directly expressible in a form similar to Eq. (67), i.e., as a polynomial in powers of Lorentzians which are readily programmable. It should be kept in mind, however, that these polynomials in L used to represent the d functions are only alternative expressions for the smooth slowly varying derivatives shown in Eq. (61).

In Fig. 5 we show $S(x)$ for the separate contributions from $j=1$, 2, and 3, which reflect the basic shape of $\mathcal{J}_j(x)$ or $d^{(0)}_j(x)$ for the terms shown in Eq. (67). Figure 5(a) shows calculated $S^{(0)}(x)$ found by numerical integration of the convolution integral. When the three contributions from $j=1$, 2, and 3 are combined the result differs from the ideal data base shown in Fig. 5(a) by the amount shown in Fig. 5(e), indicating a maximum error at $x=0$ which is only 5% from the true line shape.

As noted earlier, the power series sums shown in Eq. (61) can be carried out for practical purposes to infinity, by putting a suitable criterion on the size of successive terms. For very large t the number of terms in this sum may be very large but it is still easily evaluated. For $t=4$, summing m to 20 gives results of the accuracy shown in Figs. 5 and 6. Of more critical importance is the convergence on j. In Fig. 6 we show the difference in a carefully numerically evaluated convolution with our analytic representation for $j=4$, 6, 8, and 10. With only four terms the analytic representation is within 1% of the true line shape and is more accurate than many experiments and with six terms in j the accuracy exceeds the best experiments to date. The error with ten terms is less than 1 part in 10^6 and the graininess of the plot is the result of the finite step size used in the numerical evaluation of the convolution integral. The small negative result in the asymptotic region ($x\gg 1$) is the result of truncation of the numerical integration which in principle should be summed to infinity.

VI. INCLUSION OF INTERFERENCE IN THE DESCRIPTION OF LINE SHAPE

The Fourier transform of the convolution of the unbroadened Lorentzian source distribution and the absorption function in the absence of interference gives the line shape of the transmission signal as described in Eqs. (58), (61), and (62). The contribution from interference to order β^2 requires adding to the analysis the contributions to the integral, I_{0m}, given in Eq. (38) the linear and quadratic terms in β that result from expanding $(1-4\beta x')^m$. The first of these is linear in x' and β, and is

$$I^{(1)}_{0m}(x)=\mathcal{F}^{-1}(F^{(0)}_{0\pm}G^{(1)}_{m\pm})$$
$$=-\frac{4\beta m}{4^m}\int_{-\infty}^{\infty}\frac{x'dx'}{[(x'-x)^2+1/4](x'^2+1/4)^m}\ . \tag{68}$$

From the transforms in Table I we immediately arrived at

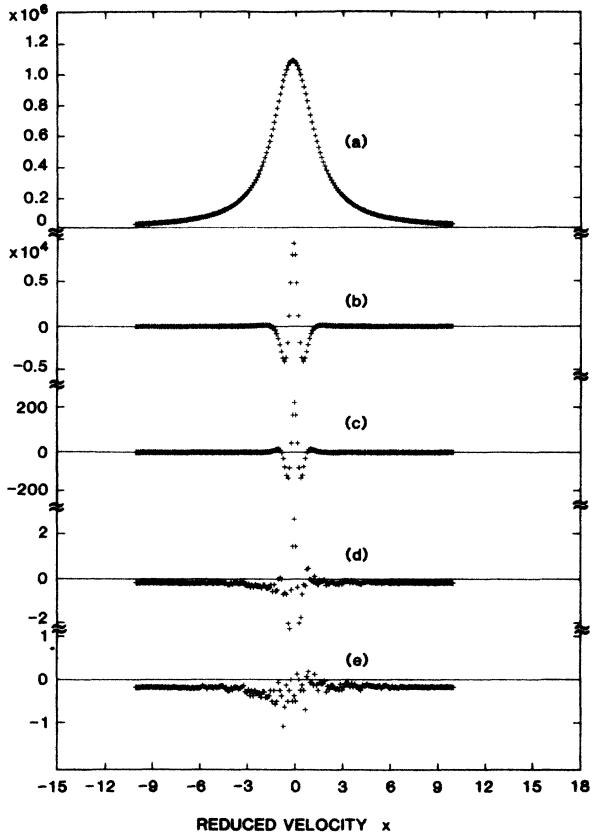

FIG. 6. (a) Computer-generated data base for $t=4$, $R_0=(\pi/2)\times 10^6$, $t_{rs}=T_{es}=\beta=0$. The error signal when progressively larger numbers of j terms are included; (b) $S_{\text{CONV}}-S_{\text{AN}}$ when four terms in j are included (1, 2, 3, and 4); (c) $S_{\text{CONV}}-S_{\text{AN}}$ when six terms in j are included; (d) $S_{\text{CONV}}-S_{\text{AN}}$ when eight terms in j are included; (e) $S_{\text{CONV}}-S_{\text{AN}}$ when ten terms in j are included. The scatter is caused by the finite steps in the numerical evaluation of the convolution signal and the displacement from zero (1 part in 10^7) is the result of the truncation of the numerical integration at large x.

$$I_{0m}^{(1)}(x)=-(4\beta m)/4^{m+1}\sum_{j=1}^{m}C_{jm}d_j^{(1)}(x)\ , \tag{69}$$

where

$$d_j^{(1)}=(j-1)\mathscr{J}_{j-1}(x)+\mathscr{J}_j(x)$$
$$=x\left[(j-1)L_{w0}^{(j-2)}+L_{w0}^{(j-1)}\right]\ . \tag{70}$$

$\mathscr{J}_j(x)$ is the rest of odd parity functions that represents the inverse transform

$$\mathscr{J}_j(x)=\frac{i}{2}\int_{-\infty}^{0}(\alpha/2)^{j-1}\exp[i\alpha x+\alpha(w+1)/2]d\alpha$$
$$-\frac{i}{2}\int_{0}^{\infty}(-\alpha/2)^{j-1}\exp[i\alpha x-\alpha(w+1)/2]d\alpha\ . \tag{71}$$

Every $d(x)$ function treated in this paper is directly derivable from the two basic sets $\mathscr{I}_j(x)$ and $\mathscr{J}_j(x)$. Since all of the convolution integrals that we will deal with have a dependence on x which can be expressed in the form shown in Eqs. (50) and (71), we give catalogs of L_w, $L_{w0}^{(j-1)}=(1/x)\mathscr{J}_j(x)$ and $\mathscr{I}_j(x)$ in Tables II and III for $j=1$ to 10.

Again the integral has a structure that permits the use of the recursion relation Eq. (65), although in this case $\mathscr{J}_1(x)=xL_{w0}=xL(x)$ in contrast to $\mathscr{I}_1(x)$, which is $(w+1)L_w$ evaluated as $w=1$, as shown in Eq. (51).

Substituting Eq. (69) into Eq. (36) gives the first-order contribution to the signal from interference, i.e.,

$$S^{(1)}(x)=f_{s0}C_0\beta\sum_{j=1}^{\infty}\sum_{m=j}^{\infty}(-4m\,A_{jm}t^m)d_j^{(1)}(x)$$
$$\equiv f_{s0}C_0\sum_{j=1}^{\infty}\beta D_j^{(1)}(t)d_j^{(1)}(x)\ . \tag{72}$$

An important point to note is that this and all subsequent expressions for $S(x)$ except for $S^{(2)}(x)$ can be written in a form similar to Eqs. (49) and (72) with propor-

TABLE II. A catalog of $L_{w0}^{(j-1)}$, which is L_w evaluated at $w=1$, and $(1/x)\mathscr{J}_j(x)$.

j[a]	$L_{w0}^{(j-1)}=(1/x)\mathscr{J}_j(x)$	Sum of coefficients[b]
1	$L(x)=(1+x^2)^{-1}$	1
2	$-L^2$	−1
3	$-0.5L^2+2L^3$	1.5
4	$3L^3-6L^4$	−3
5	$1.5L^3-18L^4+24L^5$	+7.5
6	$-22.5L^4+120L^5-120L^6$	−22.5
7	$-11.25L^4+270L^5-900L^6+720L^7$	78.25
8	$315L^5-3150L^6+7560L^7-5040L^8$	−315
9	$157.5L^5-6300L^6+37\,800L^7-70\,560L^8+40\,320L^9$	1417.5
10	$-7087.5L^6+113\,400L^7-476\,280L^8+725\,760L^9-362\,880L^{10}$	−7087.5

[a]To calculate terms beyond the $j=10$ term we need only carry out additional derivatives of the 10 terms for L_w, which is $L_w=-3543.75(w+1)L_w^6+14\,175(w+1)^3L_w^7-14\,883.75(w+1)^5L_w^8+5670(w+1)^7L_w^9-708.75(w+1)^9L_w^{10}$.

[b]To avoid errors in generating these basis functions it is helpful to notice that the sum of the coefficients of the j term is $j/2$ times the magnitude of the $j-1$ term and the sign of the sum of coefficients alternate.

TABLE III. Catalog of $\mathcal{J}_j(x)$ expressed as polynomials of powers of Lorentzians. As in Table II higher-order terms can be obtained by continuing differentiations of $L_w(x)$ and substitution in Eq. (66). Again terms can be checked by summing coefficients. In this series the sum of the coefficients of the jth term is equal to $(j-1)/2$ times the sum of the coefficients of the $j-1$ term, with successive sums having alternating signs.

j	$\mathcal{J}_j=d_j^{(0)}(x)$
1	$2L$
2	$L-2L^2$
3	$-3L^2+4L^3$
4	$-1.5L^2+12L^3-12L^4$
5	$15L^3-60L^4+48L^5$
6	$7.5L^3-135L^4+360L^5-240L^6$
7	$-157.5L^4+1260L^5-2520L^6+1440L^7$
8	$-78.75L^4+2520L^5-12\,600L^6+20\,160L^7-10\,080L^8$
9	$2835L^5-37\,800L^6+136\,080L^7-181\,440L^8+80\,640L^9$
10	$1417.5L^5-70\,875L^6+567\,000L^7-1\,587\,600L^8+1\,814\,400L^9-725\,750L^{10}$

tional coefficients. When this is done the expressions for $d_j(x)$ will always be composites of the basis functions $\mathcal{J}_j(x)$ or $\mathcal{I}_j(x)$, similar to what is shown in Eq. (70). This requires making a sum of these functions, which is most easily done using the computer.

An alternative to using Eqs. (70) and (72) is to express each contribution to $S(x)$ in terms of the basis functions $\mathcal{J}_j(x)$ or $\mathcal{I}_j(x)$, which requires taking a linear combination of coefficients and calculating with the computer the new set of coefficients for each case.

Following this alternative approach, Eq. (72) is then given by

$$S^{(1)}(x)=f_{s0}C_0\beta\sum_{j=1}^{\infty}\sum_{m=j}^{\infty}[-4m(jA_{j+1,m}+A_{jm})]\times t^m\mathcal{I}_j(x)\ . \tag{73}$$

Equations (72) and (73) are equivalent, and while the second approach has a formal elegance and reduces each expression to the minimum basis set of functions, it is more tedious to algebraically reduce the combined coefficients to their simplest form and we recommend letting the computer find these coefficients.

The second-order contribution from interference is found from the $8m(m-1)\beta^2$ term in the expansion of $(1-4\beta x')^m$ in Eq. (38).

Here we find for the inverse transform

$$I_m^{(2)}=\mathcal{F}^{-1}(F_{0\pm}^{(0)}G_{m\pm}^{(2)})=-\frac{2m(m-1)}{4^m}\sum_{j=1}^{m}C_{jm}d_j^{(2)}(x)\ , \tag{74}$$

where

$$d_j^{(2)}(x)=(j-1)(j-2)\mathcal{J}_{j-2}+2(j-1)\mathcal{J}_{j-1}+\mathcal{J}_j\ . \tag{75}$$

Substituting of Eq. (74) into Eq. (33) gives the β^2 contribution to the resonance signal, i.e.,

$$S^{(2)}(x)=f_{s0}C_0\beta^2\sum_{j=1}^{\infty}\sum_{m=j}^{\infty}[-2(m-1)mA_{jm}]t^m d_j^{(2)}(x)\ , \tag{76}$$

where $d_j^{(x)}(x)$ is given by Eq. (75).

In terms of the $\mathcal{J}_j$ basis Eq. (76) can be rewritten as

$$S^{(2)}(x)=f_{s0}C_0\beta^2\sum_{j=1}^{\infty}\sum_{\substack{m,j\\(m=j)}}^{\infty}[-2m(m-1)]\times[j(j+1)A_{j+2,m}+2jA_{j+1,m}+A_{jm}]\times t^m\mathcal{J}_j(x)\ . \tag{77}$$

Here we see an advantage of expressing the resonance signal in the form of Eq. (77) rather than (76). As we noted earlier, only $\mathcal{J}_1(x)$ will contribute to area under the resonance absorption curve. From Eq. (77) this area is immediately apparent as only the $j=1$ term contributes, and since the integral of $2L(x)$ is 2π, we find the contribution to the area under the absorption associated with $S^{(2)}(x)$ is

$$A_T^{(2)}=f_{s0}C_0\beta^2(2\pi)\sum_{m=1}^{\infty}(-2m)(m-1)A_{1m}\times[2A_{3m}+2A_{2m}+A_{1m}]t^m\ . \tag{78}$$

With some algebraic manipulation this can be shown to reduce to

$$A_T^{(2)}=f_sC_0\beta^2(2\pi)\sum_{m=1}^{\infty}\frac{2m(m-1)}{(2m-3)}A_{1m}t^m\ , \tag{79}$$

where A_{jm} is given by Eq. (60) with $j=1$. It is noteworthy that this contribution to the area is negative, i.e., interference reduces the area under the resonance signal curve. For $\beta=0.1$ as in ^{181}Ta and ^{73}Ge this can give a significant contribution, especially at large t.

VII. INCLUSION OF SOURCE SELF-ABSORPTION IN THE CONVOLUTION PROBLEM

As we show in Eqs. (18) and (26) and illustrate in Fig. 4, the spectral distribution of source emission is notice-

ably flattened for even modest source resonance self-absorption (SRSA). Such SRSA noticeably broadens and diminishes the height of the convoluted pattern that is observed in an ME experiment. It flattens the convoluted spectral distribution and usually a correction for this broadening is essential if correct t values (cross sections) and accurate width parameters are to be determined from ME data.

We can calculate most of the effect of SRSA by evaluating the second integral in Eq. (33), which is accurate to linear terms in t_{rs} as depicted in Eq. (28). Referring to this first source broadening integral as I_{1m}, in keeping with the notation of Eq. (38), the contribution to the mth term, when $g(x')$ is expanded as previously [Eq. (35)], is given by

$$I_{1m}=\frac{1}{4^{m+2}}\int_{-\infty}^{\infty}\frac{(1-4\beta X)(1-4m\beta x')dx'}{(X^2+1/4)^2(x'^2+1/4)^m} . \quad (80)$$

If we multiply the factors in the numerator and neglect terms of order $\beta^2 t_{rs}\tau_1$, then this integral can be partitioned as follows:

$$I_{1m}=I^{(1S)}+I^{(11)}+I^{(10)} , \quad (81)$$

where the superscript (1S) refers to the symmetric part of I_{1m}, (11) refers to the antisymmetric part of I_{1m} due to the linear β term in the source distribution and (10) the antisymmetric part due to the linear β term in the absorption function.

In our notation all terms with double index superscripts are terms referring to corrections due to SRSA. The first index, in this case 1, gives the value of k, which is the order of the correction. The second index S, 1, or 0 means the symmetric term, the 1 and 0 refer to the source terms which are linear in β and independent of β, respectively; i.e., the three contributions to the integrals may be written as

$$I^{(1S)}=\mathcal{F}^{-1}[F^{(0)}_{1\pm}(\alpha)G^{(0)}_{m\pm}(\alpha)] \quad (k=1, \text{ symmetric part}) ,$$

$$I^{(11)}=\mathcal{F}^{-1}[F^{(1)}_{1\pm}(\alpha)G^{(0)}_{m}(\alpha)] \quad (k=1, F^{(1)}, \text{ antisymmetry part}) , \quad (82)$$

and

$$I^{(10)}=\mathcal{F}^{-1}[F^{(0)}_{1\pm}(\alpha)G^{(1)}_{m}(\alpha)] \quad (k=1, F^{(0)}, \text{ antisymmetric part}) .$$

Again we write these integrals and their corresponding resonance signals, $S^{(1S)}_1$, $S^{(11)}_1$, and $S^{(10)}_1$ by inspection using the transform catalog in Table I. For each k there will be three terms similar to Eq. (82), but the first superscript will be changed to the value of k (order in t_{rs}) being considered.

For each value of k there will be three integrals similar to the above. For the $k=1$ terms we have

$$I^{(1S)}=\tfrac{1}{2}4^{-(m+1)}\sum_{j=1}^{\infty}C_{jm}d_j^{(1S)}(x) , \quad (83)$$

where

$$d_j^{(1S)}(x)=\mathcal{J}_j(x)-\mathcal{J}_{j+1}(x) . \quad (84)$$

When this result is substituted into Eq. (33) to get the (1S) contribution to the resonance signal, we find

$$S^{(1S)}(x)=f_{s0}C_0\tau_1 t_{rs}\sum_{j=1}^{\infty}\sum_{m=j}^{\infty}(\tfrac{1}{2}A_{jm})t^m d_j^{(1S)}(x) . \quad (85)$$

The corresponding results for the (11) and (10) terms are

$$S^{(11)}(x)=f_{s0}C_0\tau_1 t_{rs}\sum_{j=1}^{\infty}\sum_{m=j}^{\infty}(2\beta A_{jm})t^m d_j^{(11)}(x) , \quad (86)$$

and

$$S^{(10)}(x)=f_{s0}C_0\tau_1 t_{rs}\sum_{j=1}^{\infty}\sum_{m=j}^{\infty}[(-2\beta)m A_{jm}]t^m d_j^{(10)}(x) , \quad (87)$$

with

$$d_j^{(11)}(x)=\mathcal{J}_{j+1}(x) , \quad (88)$$

and

$$d_j^{(11)}(x)=(j-1)\mathcal{J}_{j-1}(x)+(2-j)\mathcal{J}_j(x)-\mathcal{J}_{j+1}(x) . \quad (89)$$

If we use Eqs. (85) to (87) to include the linear t_{rs} representation of the resonance signal, we find that the error for $t_{rs}=0.5$, $T_{es}=1$ drops from 12% to 2%, as is illustrated in Figs. 7(b) and 7(c), where Fig. 7(a) shows the computer generated data base. As the quadratic and cubic terms in t_{rs} are included the difference with our "ideal" data base drops rapidly as seen in Figs. 7(d) and 7(e). After inclusion of the cubic terms S_{AN} [Eq. (87)] agrees with S_{CONV} to nearly one part in 10^4.

The successive k values give integrals similar to those displayed in Eq. (82) and the resonance signal contribution is similar to Eqs. (83) through (85). All of the integrals and signal functions have the same basic structure, with the even parity contributions expressed in terms of the $\mathcal{J}_j(x)$ basis and the odd parity contributions expressed in terms of the $\mathcal{J}_j(x)$ functions.

In general we can write each contribution to I and S in the form

$$I^{(M)}(x)=K_m 4^{-(m+1)}\sum_{j=1}^{m}C_{jm}d_j^{(M)}(x) , \quad (90)$$

and

$$S^{(M)}(k)=f_{s0}C_0\tau_k t_{rs}^k\sum_{j=1}^{\infty}\sum_{m=j}^{\infty}K_m A_{jm}t^m d_j^{(M)}(x) , \quad (91)$$

where K_m are constant coefficients which generally have a dependence on the index m and where $d^{(M)}(x)$ is a linear combination of the $\mathcal{J}_j(x)$ functions for the even parity contributions and a linear combination of the $\mathcal{J}_j(x)$ functions for the odd parity states. The superscript (M) labels the order of the contribution. When (M) is only one index (0,1,2) then we are referring to the $k=0$ contributions from β^0,β^1,β^2, respectively. All of the con-

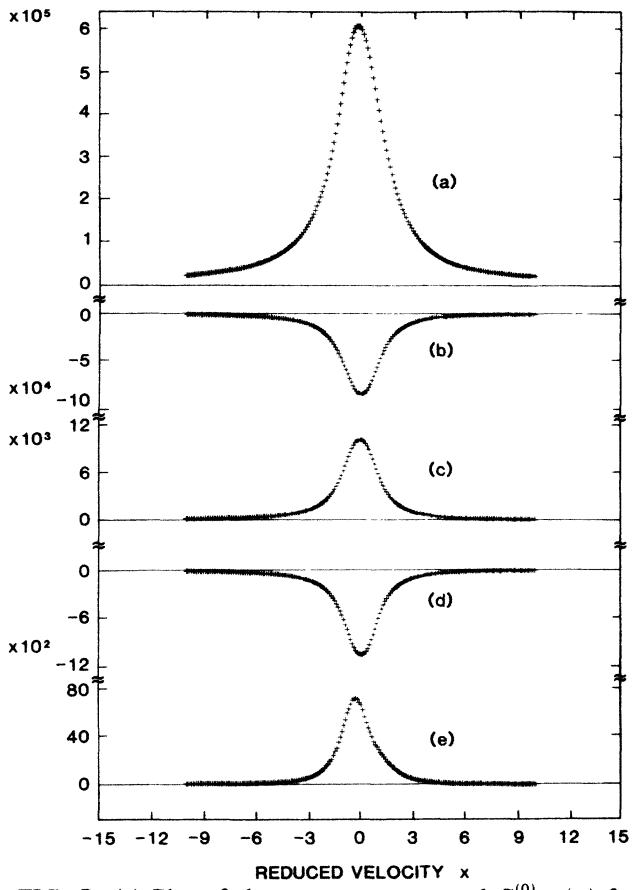

FIG. 7. (a) Plot of the computer generated $S^{(0)}_{\mathrm{CONV}}(x)$ for $t=4$, $\beta=0.01$, $t_{rs}=0.5$, $T_{es}=1$, and $f_{s0}C_0=(\pi/2)\times 10^6$. (b) Plot of $S_{\mathrm{CONV}}(x)-S_{\mathrm{AN}}(x)$ setting t_{rs} equal to zero. (c) Same as (b) but with $t_{rs}=0.5$, $T_{es}=1$, evaluating only to the linear term in t_{rs}; (d) same as (b) but with the quadratic term t_{rs}^2 included, and (e) same as (c) but with the t_{rs}^3 term added. In each case no parameters are varied.

tributions associated with source broadening $k=1,2,3\ldots$ have two indices and the first is the k value that labels explicitly the order, i.e., t_{rs}^k.

In Table IV we give the values of k_m and $d_j^{(M)}(x)$ through $k=3$. We also give a set of coefficients $A_{jm}^{(M)}$, which is related to $d_j^{(M)}(x)$, which is the set of coefficients that expresses the solution of $S^{(M)}(x)$ in terms of the basis functions $\mathcal{I}_j(x)$ and $\mathcal{J}_j(x)$ and permits area evaluation by inspection.

As noted earlier the computation of areas under the resonance curve is most easily evaluated by expressing $S(x)$ in terms of the basis Fourier transforms $\mathcal{I}_j(x)$ and $\mathcal{J}_j(x)$. When this is done the signal can always be written in the form

$$S^{(M)}(x)=f_{s0}C_0\tau_k t_{rs}^k \sum_{j=1}^{\infty}\sum_{m=j}^{\infty} K_m A_{jm}^{(M)} t^m \mathcal{I}_j(x) \tag{92}$$

for the even parity terms, and

$$S^{(M)}(x)=f_{s0}C_0\tau_k t_{rs}^k \sum_{j=1}^{\infty}\sum_{m=j}^{\infty} K_m A_{jm}^{(M)} t^m \mathcal{J}_j(x) \tag{93}$$

for the odd parity terms. Since A_{jm} is fundamentally related to the $d_j^{(M)}(x)$ functions, the $A_{jm}^{(M)}$ coefficients are obtained by the appropriate raising or lowering of the basis functions. Thus, we give the $A_{jm}^{(M)}$ coefficients for all contributions considered in this paper in the same column of Table IV as the $d_j^{(M)}(x)$ functions, which clearly reveals this interrelation.

If curve fitting is the primary goal, either form of $S(x)$ is acceptable. In the data that we display in Fig. 7, we wrote the program using the $d_j^{(M)}(x)$ function to evaluate the contributions to $S(x)$, and the curves shown were evaluated using that approach. The curves in Fig. 7 show the effect of adding on successive orders of t_{rs}. Figure 7(a) is a display of the computer-generated data base with $t_{rs}=0.5$ and $T_{es}=1$. Plots 7(b)–7(e) show, respectively, the error resulting from the analytic forms of $S(x)$ when all terms in t_{rs} are omitted, when the linear term alone is included, when the linear and quartic terms are included, and finally, when all terms through cubic are included. It is seen that the inclusion of terms through cubic is sufficient to describe the true resonance signal curve to about one part in 10^4 for source thickness number up to 0.5.

TABLE IV. K_m coefficients, d functions, and matrix coefficients for order M.

(M)	$K_m^{(M)}$	$d_j^{(M)}(x)$	$A_{jm}^{(M)}$
(0)	1	$\mathcal{I}_j(x)$	A_{jm}
(1)	$(-4\beta)m$	$(j-1)\mathcal{J}_{j-1}+\mathcal{J}_j$	$jA_{j+1,m}+A_{jm}$
(2)	$-\beta^2[2m(m-1)]$	$(j-1)(j-2)\mathcal{I}_{j-2}+2(j-1)\mathcal{I}_{j-1}+\mathcal{I}_j$	$j(j+1)A_{j+2,m}+2jA_{j+1,m}+A_{jm}$
(1S)	$\frac{1}{2}$	$\mathcal{I}_j-\mathcal{I}_{j+1}$	$A_{jm}-A_{j-1,m}$
(11)	2β	$\mathcal{J}_{j+1}$	$A_{j-1,m}$
(10)	$(-2\beta)m$	$(j-1)\mathcal{J}_{j-1}+(2-j)\mathcal{J}_j-\mathcal{J}_{j+1}$	$jA_{j+1,m}+(2-j)A_{jm}-A_{j-1,m}$
(2S)	$\frac{1}{8}$	$3\mathcal{I}_j-3\mathcal{I}_{j+1}+\mathcal{I}_{j+2}$	$3A_{jm}-3A_{j-1,m}+A_{j-2,m}$
(21)	$(-\beta)$	$-\mathcal{J}_{j+1}+\mathcal{J}_{j+2}$	$-A_{j-1,m}+A_{j-2,m}$
(20)	$(-\beta/2)m$	$3(j-1)\mathcal{J}_{j-1}+3(2-j)\mathcal{J}_j+(j-4)\mathcal{J}_{j+1}+\mathcal{J}_{j+2}$	$3jA_{j+1,m}+3(2-j)A_{jm}+(j-5)A_{j-1,m}+A_{j-2,m}$
(3S)	$\frac{1}{48}$	$15\mathcal{I}_j-15\mathcal{I}_{j+1}+6\mathcal{I}_{j+2}-\mathcal{I}_{j+3}$	$15A_{jm}-15A_{j-1,m}+6A_{j-2,m}-A_{j-3,m}$
(31)	$(-\beta/4)$	$-3\mathcal{J}_{j+1}+3\mathcal{J}_{j+2}-\mathcal{J}_{j+3}$	$-3A_{j-1,m}+3A_{j-2,m}-A_{j-3,m}$
(30)	$(-\beta/12)m$	$15(j-1)\mathcal{J}_{j-1}+15(2-j)\mathcal{J}_j+(6j-21)\mathcal{J}_{j+1}+(7-j)\mathcal{J}_{j+2}-\mathcal{J}_{j+3}$	$15jA_{j+1,m}+15(2-j)A_{jm}+(6j-27)A_{j-1,m}+(9-j)A_{j-2,m}-A_{j-3,m}$

Although almost all the authors reporting interference and line-shape parameters in the literature have used a Lorentzian fit [Eq. (5)], we see in Table V, by comparing with column b, just how unsatisfactory this is for a data base such as shown in Fig. 7(a). The parameters are completely wrong and the chi-square value is 14. A comparison of the computer-generated data base [Fig. 7(a)] with a Lorentzian fit is given in Fig. 8(a).

Another semiempirical fit to the ME line proposed by Mullen *et al.*[18] is based on an exponential Lorentzian. Here the agreement for width is much better, although the error in the interference parameter is 35% as compared to 92% for the Lorentzian fit. The chi-square value of this fit is better than the chi-square value for the analytic fit with only linear terms in t_{rs}, even though this latter case gives much more accurate line-shape parameters, as can be seen in Table V. A comparison of the computer-generated data base [Fig. 7(a)] with the exponential-Lorentzian function (ELF) is shown in Fig. 8(b). Some of the parameters like interference are not in good harmony with the true values, but others like width agree very well. The computer time for the ELF fit and the Lorentzian fit is orders of magnitude less than the full analytic function, although it is certainly not prohibitive for the analytic form.

In Fig. 8 we find a remarkable fact about our solution. If we curve fit with the t_{rs} linear term included to the data base shown in Fig. 7(a), we find that the chi-square fit is better without including the t_{rs} term [Fig. 8(c)] than it is with the linear t_{rs} correction included [Figs. 8(d) and 8(e)]. When t_{rs} is allowed to vary it gives a better fit [Fig. 8(d)] as expected than when it is not [Fig. 8(e)]. The important point to note, however, is that the accuracy of the fitted parameters is in an inverse relation with the chi-square value given for the fit. This is clearly revealed in Table V, where we display the fitted parameters for the three cases. In columns c, d, and e the chi-square values get progressively worse while the accuracy of the parameters get progressively better, completely at variance with the conventional wisdom in the field that a good chi-square value means a good fit, which implies correct parameters.

While this at first glance appears to be a paradox, the origin of the result is clear when we look at Eqs. (38)–(43). We see that the functional forms of the source and absorber transforms are the same except for step-up factors. Thus it is extremely difficult for a computer fit to give the correct line-shape parameters unless t_{rs} is known by an independent determination.

Notice that the "best fit" for the computer-generated data base shows only 50 ppm maximum deviation from the true $S(x)$ when t_{rs} is taken as zero instead of the correct input value of 0.5, which is well beyond experimental detection.

When the analytic form of $S(x)$ is extended to include t_{rs}^3 terms, it then gives both a better chi-square value and the correct parameters. In this case the deviation from the true $S(x)$ is less than 10 ppm and the output parameters are almost exact. It must be emphasized, however, that even if cubic terms are included when real data are analyzed, it is not possible for the computer to get reliable t_{rs} values with data of even relatively good precision, since no one yet has been able to accumulate count statistics of such precision that the standard deviation of the resonance signal is of order 10 ppm.

In Sec. VII we discuss ways of independently determining t_{rs} so that it can be fixed in the data analysis and the correct line-shape parameters found from the experimental data. It should be mentioned here, however, that the biggest errors in line-shape parameters that occur, as can

TABLE V. Mössbauer parameters determined by a least-squares fit to a computer-generated data base. Columns c through h correspond to the results shown in Figs. 8(a) through 8(f) compared to the computer-generated data base shown in Fig. 7(a).

a	b	c	d	e	f	g	h
v_0	0	1.20×10^{2}	1.86×10^{-3}	9×10^{-4}	-1.4×10^{-5}	-7.3×10^{-5}	-2.5×10^{-6}
Γ_M	1.0	1.55	1.06	1.052	1.008	0.999	0.9998
t	4.0			3.77	3.93	3.95	4.001
h[i]	1.0			0.94	0.99	1.02	0.998
β	10^{-2}	1.92×10^{-2}	1.35×10^{-2}	1.02×10^{-2}	1.01×10^{-2}	1.00×10^{-2}	1.00×10^{-2}
t_{rs}	0.5			0 fixed	0.403	0.5 fixed	0.500
T_{es}	1.0			1.0 fixed	1.0 fixed	1.0 fixed	1.0 fixed
χ^2		14.5	4.9×10^{-3}	2.96×10^{-4}	2.04×10^{-3}	2.42×10^{-3}	1.50×10^{-5}
$S(x)$	0	1.32×10^{-3}	1.56×10^{-5}	0	0	0	0

[a]Parameter label.

[b]Input value for parameter in determining the computer-generated data base.

[c]Comparison of a Lorentzian fit [Eq. (5)] with "ideal" data base.

[d]Comparison of an exponential-Lorentzian fit (Ref. 18) to the ideal data base.

[e]Parameters determined by fit of $S_{AN}(x)$ with t_{rs} taken as zero in analytic form with all parameters except T_{es} and t_{rs} varied. $S_{AN}(x)$ is the analytic form given in Eq. (91).

[f]Parameters determined by fit of $S_{AN}(x)$ with only linear t_{rs} terms included to ideal data base, with all parameters except T_{es} varied.

[g]Same as d, but with t_{rs} fixed at the correct value of 0.5, with all parameters except T_{es} and t_{rs} varied.

[h]Same as d, but including quadratic and cubic t_{rs} terms in analytic representation.

[i]h is a height factor reflecting the error in $f_{s0}C_0$, i.e., $h=1$ would correspond to the fitted value being the same as the input value used to generate the "ideal" data base.

be seen by examining Table V, are the errors in t (or cross section) and height gauge, $f_{s0}C_0$. If t is determined independently by first using a source with negligible SRSA, then the least-squares fit procedure will give much more reliable values of t_{rs}. The reason is again that SRSA leads to the same functions in the convolution integrals [Eq. (38)] as resonance absorption in the absorber.

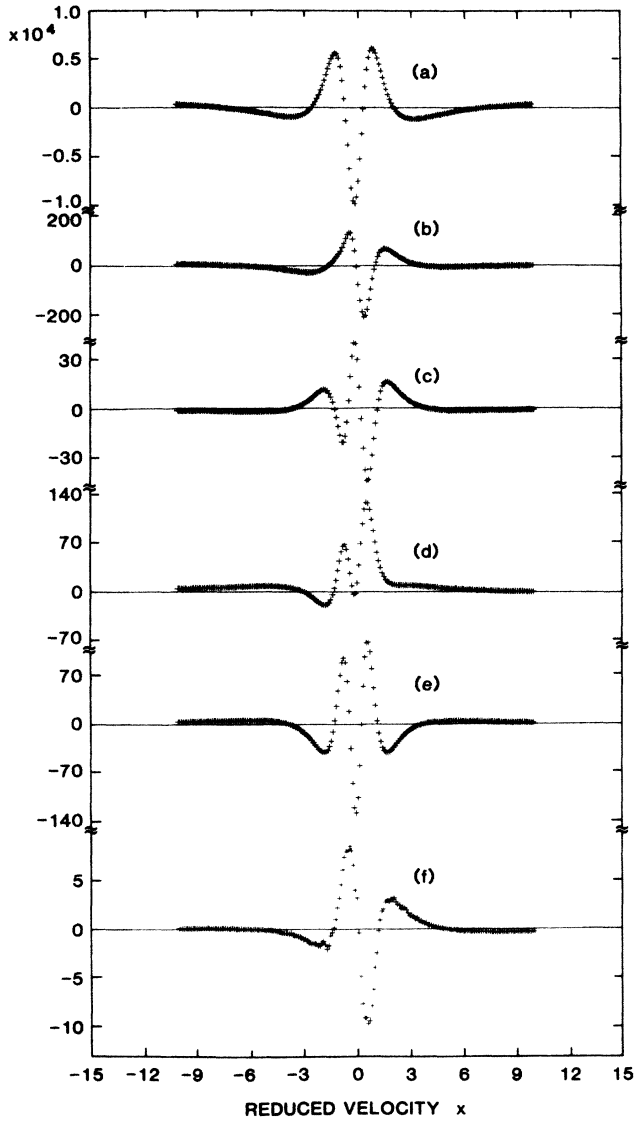

FIG. 8. Error signals for various orders of refinement of the analytic representation of the convolution integral when the parameters are set by least-squares fitting to the "perfect" data base, displayed in Fig. 7(a). (a) $S_{\mathrm{CONV}}-S_{\mathrm{LOR}}$; (b) $S_{\mathrm{CONV}}-S_{\mathrm{ELF}}$; (c) $S_{\mathrm{CONV}}-S_{\mathrm{AN}}$ with t_{rs} set equal to zero; (d) $S_{\mathrm{CONV}}-S_{\mathrm{AN}}$ with $t_{rs}=0.5$ including $k=0,1$ (up to linear t_{rs} terms), with all parameters allowed to vary; (e) same as (d) but t_{rs} fixed at correct value; (f) $S_{\mathrm{CONV}}-S_{\mathrm{AN}}$ with t_{rs} terms through t_{rs}^3 included and allowed to vary as independent parameters. In this analysis for (b)–(e) all parameters, including Γ_M, t, $f_{s0}C_0$, and v_0, are varied to give the best possible fit to the "ideal" data base determined by a numerical integration of the convolution integral with the parameters $t=4$, $\beta=0.01t_{rs}=0.5$, $T_{es}=1$, and $f_{s0}C_0=(\pi/2)\times 10^6$. The one exception was T_{es}, which was always set equal to 1, as this parameter is usually extremely easy to obtain by an independent thickness measurement.

VIII. AREAS AND PEAK HEIGHTS OF TRANSMISSION SPECTRA

Bykov and Hien[5] have shown that for a single line resonance the area and peak height are functions of the absorption thickness, expressing their results in terms of modified Bessel functions. With the present analysis we can make an important generalization of their result, including the effects of interference and source self-absorption. Their result is equivalent to our Eq. (63) for the area under the resonance transmission curve when $\beta=t_{rs}=0$.

Since $S^{(1)}(x)$ contains only odd functions of x, i.e., $d_j^{(1)}(x)=-d_j^{(1)}(-x)$, the linear terms in β reflected in $S^{(1)}(x)$ will not contribute to the area. The terms in $S^{(2)}$ are even, however, and they will contribute to the area terms of order β^2. Only terms which cannot be expressed as derivatives with regard to x contribute to the area, and these are most easily identified when $S^{(M)}(x)$ is written in the form of Eqs. (92) and (93), i.e., in terms of the basis functions $\mathcal{J}_j(x)$ and $\mathcal{J}_j(x)$. When this is done the only term which contributes to the area is the $j=1$ term. Since the $\mathcal{J}_j(x)$ terms are of odd parity none of these terms contribute and only $\mathcal{J}_1(x)$ makes a contribution of 2π. An examination of Table IV reveals the terms in (M) which contribute are (0), (2), (1s), (2s), and (3s).

Combining $(M)=(1s)$, $(2s)$, and $(3s)$ contributions from SRSA with the results in Eqs. (63) and (79), and further noting that each of these contributions would have the same β^2 reduction had we expanded the absorption terms to order β^2 and included them in the calculation of $S(x)$, we have for the area under the absorption curve

$$A_T=\rho f_{s0}C_0(2\pi)\times\sum_{m=1}^{\infty}A_{1m}t^m\{1+[2m(m-1)/(2m-3)]\beta^2\}\,, \tag{94}$$

where ρ is the same reduction factor encounted in Eq. (31), written there to all orders in k, and where A_{1m} is given by Eq. (60) with $j=1$. This is not surprising as the origin of these terms arises from the reduction in area under the source spectral distribution when there is significant SRSA.

We have not been able to find any case where the term ρ has been taken into account in area measurements of recoilless fraction. Thus, these measurements are determining ρf_{s0} although they are always treated as though the measurement was of f_{s0}, which is the quantity discussed in theory.

To give some idea of the magnitude and importance of the ρ correction, consider a 100-mCi carrier-free ^{57}Co source, which has decayed for one year. It will have built up ^{57}Fe in this time sufficient to increase t_{rs} from zero to 0.3. If $T_{es}=1$, $\tau_1=-0.418$, $\tau_2=0.127$ and A_T for the same source absorber combination will have reduced 6% during the one year of usage, yet this correction has never been included in measurements of recoilless fraction based on area determination.

In Fig. 9 we show the area under the resonance signal

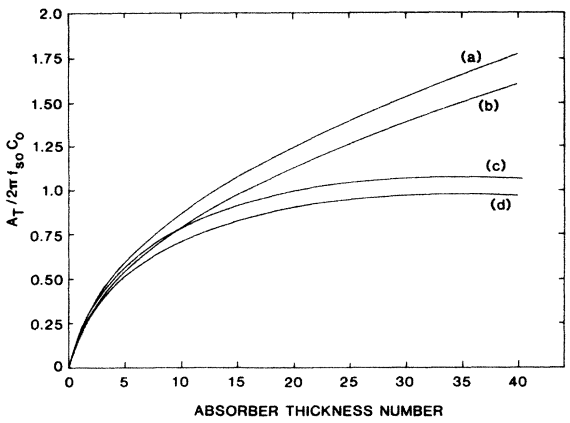

FIG. 9. Plot of the total area under the resonance-absorption curve divided by $2\pi f_{s0}C_0$ as a function of absorption thickness number t, using Eq. (94) for the following cases: (a) $\beta=0$, $t_{rs}=0$; (b) $\beta=0$, $t_{rs}=0.5$; (c) $\beta=0.1$, $t_{rs}=0$; (d) $\beta=0.1$, $t_{rs}=0.5$. (T_{es} has been taken as 1 for all cases.)

curves in units of $2\pi f_{s0}C_0$ as a function of t for $\beta=0$, $t_{rs}=0$, $\beta=0.1$, $t_{rs}=0$, $\beta=0$, $t_{rs}=0.5$, $\beta=0.1$, and $t_{rs}=0.5$. When β is as large as 0.1 as in ^{181}Ta and ^{173}Ge we find about a 1% decrease in area for each additional thickness number.

Both of the terms, which have been neglected in all past treatment of this problem can contribute significantly as we illustrate in Fig. 9. For $\beta=0.1$, $t_{rs}=0$ similar to ^{181}Ta and ^{73}Ge we find a 10% reduction in the area under the resonance curve compared to what would be expected if $\beta=0$. When there is appreciable SRSA, such as $t_{rs}=0.5$, $T_{es}=1$, we find a further reduction in area of 9% in the area under the absorption peak at all thicknesses.

Another quantity which is affected by interference and SRSA is the height of the resonance peak. All odd parity terms in S vanish at $x=0$. The contribution from $(M)=(0)$, (2), $(1s)$, $(2s)$, and $(3s)$ is given by direct application of the residue theorem, without the need for Fourier transformation. For the case where $x=0$, Eq. (38) becomes

$$I_{km}(0)=4^{-(m+k+1)}\int_{-\infty}^{\infty}\frac{(1+4\beta x)^k(1-4\beta x)^m dx}{(x^2+1/4)^{m+k+1}} . \tag{95}$$

Expanding to quadratic terms in β, using the theory of residues, and closing the contour integral on the upper half plane gives

$$I_{km}(0)=\frac{2\pi}{4^{m+k+1}}\frac{[2(m+k)]!}{[(m+k)!]^2}\times\left[1+\frac{8m(m-1)+8k(k-1)-16km}{2(m+k)-1}\beta^2\right] . \tag{96}$$

To the order of accuracy discussed in this paper this can be much simplified by considering only $k=0$, 1, 2, and 3 for the interference-free terms and take only $k=0$ for the β^2 term. This yields with Eq. (36) the result for the resonance signal at $x=0$

$$S(0)=f_{s0}C_0\sum_{m=1}^{\infty}\frac{(-1)^{m+1}(2m)!t^m}{(m!)^3}\left[1+\frac{2m+1}{2(m+1)}\tau_1 t_{rs}+\frac{(2m+1)(2m+3)}{4(m+1)(m+2)}\tau_2 t_{rs}^2+\frac{(2m+1)(2m+3)(2m+5)}{6(m+1)(m+2)(m+3)}\tau_3 t_{rs}^3+\beta^2\frac{2m(m-1)}{2m-1}\right] . \tag{97}$$

For $t_{rs}=\beta=0$ this result is again identical to that of Bykov and Hien.[5] Here, however, we see that the peak height is very sensitive to SRSA and rapidly drops off as t_{rs} increases.

In Fig. 10 we show a plot of the effect of interference and SRSA on peak height for $\beta=0.1$ and $t_{rs}=0.5$, and in Table VI we give the values of $S(0)/f_{s0}C_0$ for t and t_{rs} up to 8 and 0.5, respectively. Note that for a typical ME experiment where $t=4$ the peak height is reduced over 12% when $t_{rs}=0.5$, yet this large effect has not been included in the analysis of ME spectra.

These corrections are increasingly important as the precision of lineshape determination increases. Source parameters like t_{rs} may be time dependent. With high intensity sources of ^{183}Ta we find that t_{rs} can vary from 0.2 to 0.3 during the one week that the 5-day half-life source is used. This means that precision scattering experiments using on-resonance off-resonance counting will need time-dependent corrections for source line broadening. It is interesting that these corrections, which are in some cases quite significant, have never been made in the analysis of data to date.

It should be mentioned that the small reduction in the signal height at $x=0$, the true peak position, should not

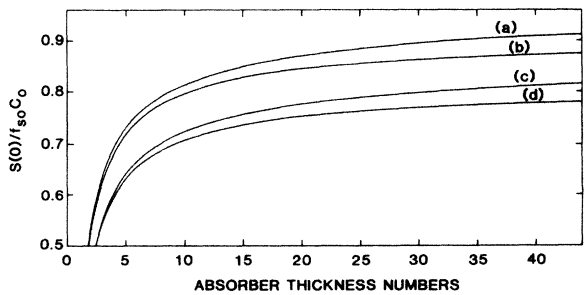

FIG. 10. Plot of the peak height under the resonance-absorption curve divided by $f_{s0}C_0$ as a function of thickness number t, using Eq. (97) for the following cases: (a) $\beta=0$, $t_{rs}=0$; (b) $\beta=0.1$, $t_{rs}=0$; (c) $\beta=0$, $t_{rs}=0.5$; (d) $\beta=0.1$, $t_{rs}=0.5$. (T_{es} has been taken as 1 for all cases.)

TABLE VI. Relative peak height at resonance, $S(0)/f_{s0}C_0$, as a function of t_{rs} and t.

t	$S(0)/f_{s0}C_0$ $t_{rs}=0$	$t_{rs}=0.25$	$t_{rs}=0.5$
0	0	0	0
1	0.355	0.330	0.307
2	0.534	0.498	0.465
3	0.632	0.591	0.553
4	0.691	0.648	0.606
6	0.757	0.710	0.667
8	0.793	0.745	0.702

be confused with the change in peak height at the peak maximum, which as we show in the next section actually increases in the thin absorber limit, when interference is present.

IX. LINE-SHAPE ASYMPTOTICS AND SHIFT IN THE SPECTRAL MAXIMUM

The analyses that have been given here have been for single unsplit lines, although they can be extended to include hyperfine split spectra. The question naturally arises, "What if it is not possible to produce an unsplit line?" In nature all crystals have impurities and vacancies and dislocations which can produce a variety of electric field gradients, broadening what would otherwise be an unsplit line.

Actually, broadening functions which have a Gaussian structure could be folded nicely into the above theory and the broadening function itself extracted from the data. Here we merely want to point out that for short-ranged broadening functions it is possible to extract the line-shape by a systematic truncation of center data and thereby extract the correct line-shape parameters such as width, interference parameter, and cross section.

A simple argument can be used to show that small hyperfine broadening does not alter the line shape in the asymptotic region. Suppose we consider two unresolved peaks whose positions are at $x=\pm\epsilon$ in the absorption term. The absorption function $g(x')$ will then be

$$g(x')=1-\exp(-\tfrac{1}{2}t\{\mathcal{L}[2(x'+\epsilon)+\mathcal{L}[2(x'-\epsilon)]\}) \ . \tag{98}$$

When this exponent is expanded in a power series in ϵ/x', all linear terms cancel and one is left with the same result as given in Eq. (13).

Thus when

$$(\epsilon/x)L \ll 1 \quad \text{or} \quad x \gg \epsilon \ , \tag{99}$$

the line shape will be the same as given in the above analysis even in the presence of unknown hyperfine or instrumental broadening. This argument can be generalized, but the bottom line result is that the asymptotic form is the same.

It should be noted that the far asymptotic region, where $S(x)$ is proportional to $1/x$, is too far removed to be of much consequence, as it is for practical purposes experimentally inaccessible. The near asymptotic region where $x \gtrsim 1$ is of much greater interest as experiments are easily carried out with the velocity range $x=\pm 6$. The exact analytic representation of the line shape means that a systematic truncation of center data can be carried out and the analytic $S(x)$ fitted to the asymptotic region considered.

For fitting of data in the asymptotic region a somewhat more efficient fitting to the line can be achieved by expressing our results as a power series of Lorentzians. Since the $d_j(x)$ are linear combinations of powers of Lorentzians this reconstruction is straightforward and can be expanded as

$$S(x)=f_{s0}C_0\sum_{j=1}^{\infty}[\lambda_j^{(0)}(t)L^j(x)+\beta\lambda_j^{(1)}(t)xL^j(x) +\beta^2\lambda_j^{(2)}(t)L^j(x)] \ , \tag{100}$$

where we have taken the source broadening terms to be negligible, and $L^j(x)=(1+x^2)^{-j}$, i.e., superscript j's in Eq. (100) refer to powers of Lorentzians.

The λ_j's are linear combinations of the D_j's and can readily be found by expressing the D_j's as powers of Lorentzians. The lowest-order terms are

$$\lambda_1^{(0)}=2D_1^{(0)}+D_2^{(0)}=\tfrac{1}{2}t+\sum_{m=2}^{\infty}\tfrac{1}{2}A_{1m}t^m \ , \tag{101}$$

$$\lambda_2^{(0)}=-2D_2^{(0)}-3D_3^{(0)}-\tfrac{3}{2}D_3^{(0)} \ ,$$

or

$$\lambda_2^{(0)}=-\tfrac{1}{8}t^2+\tfrac{1}{64}t^3+\sum_{m=4}^{\infty}A_{1m}3(m-1)/[2(2m-3)]t^m \ , \tag{102}$$

$$\lambda_1^{(1)}=D_1^{(1)}+D_2^{(1)}=-t \ , \tag{103}$$

where $D_j^{(0)}(x)$ is given in Eq. (59) and $D_j^{(1)}(x)$ by the parenthetical term in Eq. (72) summed on m.

If $x>3$, only 4 terms ($N_j=4$) are needed to represent the line shape to better than 1%. It is interesting to note that Eq. (103) does not have any quadratic or higher powers of t, which is the result of a perfect cancellation of these terms.

It should be mentioned that Eq. (100) is not the best way to fit the total pattern as its convergence in j is less optimal than the expressions found directly from the Fourier transforms, i.e., the $d_j(x)$ arising from the transforms are a much better set of basis functions for describing the line shape than the power series of Lorentzians. In fact once the general $S(x)$ is entered into the computer it is quite adequate to handle the asymptotic region, although the computer time for fitting may be slightly increased.

Equation (100) is useful for representing the shift in the resonance maximum relative to the true position, $x=0$. Since the thin limit value of this shift is $x=-\beta$, which is only 0.1 for the largest known ME transition, we may take

$$L^j(x)\cong 1-jx^2, \quad x \ll 1 \tag{104}$$

leading to the first-order result in x and β of

$$x_{\max}=\left[\sum_{j=1}^{\infty}\lambda_j^{(1)}(t)\right]\Big/\left[\sum_{j=1}^{\infty}2j\lambda_j^{(0)}(t)\right]. \tag{105}$$

Equation (105) indicates that the maximum is at $-\beta$ in the $t\ll 1$ limit and increases as the thickness number increases. Equation (105) is very poorly convergent for large t at small x. In this region Eqs. (91)–(93) are a much more rapidly convergent representation of the transmission signal $S(x)$.

For the very thin limit ($t\ll 1$), we can use Eqs. (105) and (100) to show that at the maximum in $S(x)$ the effect of interference is to increase the resonance signal at the resonance maximum, even though $S(0)$ decreases. Thus, from Eq. (105), we find for $t\ll 1$ that $x_{\max}=-\beta$, and from Eq. (100), we find $S(x_{\max})=\frac{1}{2}f_{s0}C_0t(1+\beta^2)$, while in this same thin limit $S(0)=\frac{1}{2}f_{s0}C_0t(1-\beta^2)$. Thus if we think of the interference term as being switched on then the effect is to increase the peak height of the resonance signal at the maximum by the same amount that $S(0)$ is decreased at the true peak position. For very large t (>10) this maximum in the peak height is actually less than the interference-free height. The most important point of note is that $S(0)$ and $S(x_{\max})$ change only slightly as a function of β, although they are extremely sensitive to changes in t_{rs}.

X. SUMMARY AND CONCLUSIONS

We have derived an analytic expression for the resonance signal observed in a saturation-broadened ME transmission experiment which is easily put into a computer and allows the calculation of line-shape parameters to arbitrary accuracy, including interference, width, position, and cross section. We have found this procedure allows accurate fits to transmission spectra for ^{183}W and ^{182}W and gives true line-shape parameters rather than limits, when a systematic truncation of center data is carried out and fits made to the asymptotic region ($x>1$). The transmission resonance signal, $S(x)$, is described by a highly convergent series given by Eq. (91) or alternatively by Eqs. (92) and (93). Our description is accurate to β^2 in interference and t_{rs}^3 in source self-absorption, and can be easily expanded to still higher orders if required.

The procedure also gives analytic forms for the Fourier transforms of the source and absorption terms in the transmission function (see Table I) and allows an improved deconvolution of the source and absorption spectra, which has been discussed from a strictly numerical approach by Dibar, Ure, and Flinn.[14]

In the experimental determination of line-shape parameters, much of which is summarized in Refs. 11 and 12, most of the measurements have been done using a thin limit expression for the resonance signal [see Eq. (5)], even though accurate transmission experiments can never be done in the thin limits. Some hilarious comments on this point are given in Ref. 12, giving a rather candid critique of the experimental situation. A much better empirical representation of line shape is the exponential-Lorentzian function (ELF) put forward in a recent paper by Mullen *et al.*,[18] although this approach is also only an approximate form for the line resonance signal $S(x)$.

We have shown that the area under the resonance curve depends on both the resonance self-absorption in the source and the interference parameter and we have given an explicit formula [Eq. (94)] for this dependence. It is shown that when $t_{rs}=0.5$ the recoilless fraction leaving the source is about 10% less the value when $t_{rs}=0$.

Similarly, we derived a formula [Eq. (97)] for the dependence of the resonance peak height on the source line broadening and the interference parameter. In this case the peak height is extremely sensitive to the source self-absorption, so much so that on-off experiments of resonance scattering generally need to be corrected for this term, even though it has never been considered in analyzing experimental data to date.

We have shown that the line shape in the asymptotic region will not be affected by short-range hyperfine broadening or source broadening. A special relation for the asymptotic region is given in Eq. (100) which allows a good representation in the region $x>3$ with only four terms. The general formula for $S(x)$ [Eqs. (91), or (92) and (93)] can also be used to fit data in the asymptotic region by a systematic truncation of center data and thereby eliminate short-range broadening functions which can modify the true line-shape parameters.

Note added in proof. There is a simple recursion relation for generating the $\mathcal{I}_j$ and $\mathcal{J}_j$ integrals displayed in Tables III and II, respectively.[19] The jth integral of either $\mathcal{I}$ or $\mathcal{J}$ can be expressed in terms of the two previous integrals through the relations

$$\mathcal{I}_j(x)=(1-j)L(x)[\tfrac{1}{4}(j-2)\mathcal{I}_{j-2}(x)+\mathcal{I}_{j-1}(x)]$$

and

$$\mathcal{J}_j(x)=(1-j)L(x)[\tfrac{1}{4}(j-2)\mathcal{J}_{j-2}(x)+\mathcal{J}_{j-1}(x)]\ .$$

Thus all $\mathcal{I}_j(x)$ and $\mathcal{J}_j(x)$ to any order can be calculated directly by the computer with these simple recursion relations, which eliminates the need to program into the computer the explicit funtional forms for $\mathcal{I}_j$ and $\mathcal{J}_j$, beyond the $j=1$ and $j=2$ values, which are given in the first two rows of Tables III and II, respectively.[20]

ACKNOWLEDGMENTS

We thank Qian-Yan Xi for her assistance in programming some of the convolution integrals evaluated in the early stages of this investigation. This work was prepared with the support of the U.S. Department of Energy, Grants No. DE-FG02-85 ER 45199 and DE-FG02-85 ER 45200. J.G.M. was partially supported by the University of Missouri Research Reactor Facility.

APPENDIX A

This appendix consists of a compendium of definitions used in this paper and frequently used formulas.

Parameter	Definition
τ	Mean nuclear lifetime for the ME transition being investigated
E_0	Transition energy of ME gamma transition
E_r	Relative shift of absorber compared to source due to chemical and temperature differences in source and absorber
$E=(v/c)E_0$	Doppler shift in energy of source with regard to absorber
$\Gamma_M=2\hbar/\tau$	Ideal ME width in thin absorption limit
$x=(E-E_r)\tau/\hbar$	Dimensionless gauge of velocity or energy relative to the resonance center
x'	Dimensionless gauge of velocity, or energy, used to sum the source to absorber overlap and determine the convolution of the source to absorber for a particular x
X	$x-x'$
f_{s0}	Recoilless fraction emitted from a source having no source resonance self-absorption
f_a	Recoilless fraction emitted from an absorber
f_s	Actual fraction of recoilless photons emitted from a source in the beam direction including source resonance self-absorption
SRSA	Source resonance self-absorption
ρ	f_s/f_{s0}
C_b	Count rate at detector before absorber is inserted in beam (see Fig. 2)
$R_b=f_sC_b$	Count rate at detector due to recoilless radiation
$N_b=(1-f_s)C_b$	Count rate at detector due to radiation with recoil
$A(x)$	Resonance absorption as a function of x
$A_0=-[1-\exp(-T_{ea})]R_b$	Off-resonance absorption of resonance radiation
$A_n=[1-\exp(-T_{ea})]N_b$	Off-resonance absorption of nonresonance radiation
$C(x)$	Count rate at detector when absorber is in the beam moving at reduced velocity x with regard to source
$R(x)$	Transmitted resonance count rate through absorber
$N=[\exp(-T_{ea})]N_b$	Transmitted nonresonance count rate through absorber registered at the detector
$S(x)=A(x)-A_0$	Resonance signal registered at the detector
b	Branching ratio
I_e	Nuclear spin of excited state
I_g	Nuclear spin of ground state
α	Internal conversion coefficient
λ	Wavelength of the resonance radiation
β	Interference parameter
σ_{ei}	Photoelectric plus Compton cross section for ith type atoms
σ_{es}	$\sum_{i=1}^{N_s}\sigma_{ei}a_{si}$
σ_{ea}	$\sum_{i=1}^{N_a}\sigma_{si}a_{ai}$
σ_0	Resonance cross section $\lambda^2(2I_e+1)b/[2\pi(2I_g+1)(1+\alpha)]$
$\sigma_{ra}(x)$	$f_a\sigma_0 a_{a1}\mathcal{L}(2x)$
$\sigma_{rs}(x)$	$f_s\sigma_0 a_{s1}\mathcal{L}(2x)$
n_s	Total number of atoms of all types in source per unit area
n_a	Total number of atoms of all types in absorber per unit area
a_{si}	Fraction of atoms in source of type i

a_{s1}	Fraction of atoms in source of the ME type causing self-absorption
a_{ai}	Fraction of atoms in absorber of type i
a_{a1}	Fraction of atoms in absorber of the ME type causing resonance absorption
$t_{rs}=f_s\sigma_0 a_{s1} n_s$	Thickness number for source
$t=f_a\sigma_0 a_{a1} n_a$	Thickness number for absorber
$T_{es}=\sigma_{es} n_s$	Thickness number for electronic absorption in source ($1/e$ transmission length in dimensionless form)
$T_{ea}=\sigma_{ea} n_a$	Thickness number for electronic absorption in the absorber
$L(x)$	$(x^2+1)^{-1}$
$\mathcal{L}(x)$	$(1-2\beta x)L(x)$
$L_w(x)$	$[x^2+(w/2)^2]^{-1}$
$E_k(T_{es})$	$\sum_{m=k+1}^{\infty}(-1)^{(m+1)}(m!)^{-1}\begin{bmatrix} m-1 \\ k \end{bmatrix} T_{es}^{(m-1-k)}$
$\tau_k(T_{es})$	$E_k(T_{es})/E_0(T_{es})$
C_{jm}	$\dfrac{2\pi(-2)^{j-1}(2m-j-1)!}{(m-1)!(m-j)!(j-1)!}$
A_{jm}	$\dfrac{(-1)^{m+j}2^{j-1}(2m-j-1)!}{4^m m!(m-1)!(m-j)!(j-1)!}$
$A_{j,m+1}$	$-\dfrac{(2m+1-j)(2m-j)}{4m(m+1)(m+1-j)}A_{jm}$

[1]S. Margulies and J. R. Ehrmen, Nucl. Instrum. Methods **12**, 131 (1961).

[2]S. L. Ruby and J. M. Hicks, Rev. Sci. Instrum. **33**, 27 (1962).

[3]H. Frauenfelder, D. E. Nagle, R. D. Taylor, D. R. F. Cochran, and W. M. Visscher, Phys. Rev. **126**, 1065 (1962).

[4]G. A. Bykov and P. Z. Hien, Zh. Eksp. Teor. Phys. **43**, 906 (1962) [Sov. Phys.—JETP **16**, 646 (1963)].

[5]D. A. O'Connor, Nucl. Instrum. Methods **21**, 318 (1963).

[6]J. Heberle, Nucl. Instrum. Methods **58**, 90 (1968).

[7]J. Heberle and S. Franco, Z. Naturforsch. **23a**, 1439 (1968).

[8]S. Franco and J. Heberle, Z. Naturforsch. **25a**, 134 (1970).

[9]B. T. Cleveland and J. Heberle, Phys. Lett. **40A**, 13 (1972).

[10]S. Morup and E. Both, Nucl. Instrum. Methods **124**, 445 (1975).

[11]H. C. Goldwire and J. P. Hannon, Phys. Rev. B **16**, 1875 (1977).

[12]B. R. Davis, S. E. Koonin, and P. Vogel, Phys. Rev. C **22**, 1233 (1980).

[13]J. P. Hannon and G. T. Trammell, Phys. Rev. Lett. **21**, 736 (1968).

[14]M. C. D. Ure and P. A. Flinn, *Mössbauer Methodology* (Plenum, New York, 1971), Vol. 7, p. 245.

[15]S. Nikolov and K. Kantchev, Nucl. Instrum. Methods A **256**, 161 (1987).

[16]K. Kantchev and S. Nikolov, Nucl. Instrum. Methods A **256**, 168 (1987).

[17]H. Bokemeyer, K. Wohlfahrt, E. Kankeleit, and D. Eckardt, Z. Phys. A **274**, 305 (1975).

[18]J. G. Mullen, A. Djedid, C. Holmes, G. Schupp, L. Crow, and W. Yelon, Nucl. Instrum. Methods Phys. Res. B **14**, 323 (1986).

[19]We would like to thank Bruce Bullard for calling this to our attention.

[20]Interested readers may obtain from us the functions which we have used for the resonance signal, with accompanying documentation to our program, on either magnetic tape or floppy disc.